Dalton Transactions

PAPER

View Article Online
View Journal | View Issue

Cite this: *Dalton Trans.*, 2026, **55**, 1417

Effect of combining 1-naphthoate and pentafluorobenzoate anions in Eu(III) compounds on their structure and photoluminescent properties

Anastasia A. Levina,[a,b] Maxim A. Shmelev,*[a] Andrey V. Lalov,[b] Aleksandr S. Chistyakov,[a] Julia K. Voronina,[a] Evgeniya A. Varaksina,[a,c] Ilya V. Taydakov,[c] Alexey A. Sidorov[a] and Igor L. Eremenko[a]

Received 7th November 2025,
Accepted 16th December 2025

DOI: 10.1039/d5dt02665b

rsc.li/dalton

The example of mixed-anion europium complexes containing pentafluorobenzoate (pfb), 1-naphthoate (1-nap) anions, with 1,10-phenanthroline (phen) or 2,2′-bipyridyl (2,2′-bpy) molecules demonstrates that varying the ratios of the starting reagents, as well as the conditions of synthesis and crystallization, allows for targeted control over the composition and structure of the resulting compounds: $[Eu_2(phen)_2(1\text{-nap})_4(pfb)_2]\cdot 2MeCN$ (**1**), $[Eu_2(H_2O)_2(phen)_2(1\text{-nap})_2(pfb)_4]\cdot 2MeCN$ (**2**), $[Eu_2(2,2'\text{-bpy})_2(1\text{-nap})_2(pfb)_4]\cdot 2MeCN$ (**3**), $[Eu_2(2,2'\text{-bpy})_2(1\text{-nap})_3(pfb)_3]\cdot 2MeCN$ (**4**), $[Eu_2(2,2'\text{-bpy})_2(1\text{-nap})_2(pfb)_4]\cdot 2C_6H_6$ (**5**), $[Eu_4(phen)_4(1\text{-nap})_1(pfb)_{11}]_n\cdot n[Eu_2(phen)_2(1\text{-nap})_{2.7}(pfb)_{3.3}]$ (**6**), $[Eu_2(phen)_2(pfb)_6]_n\cdot 2nMeCN$ (**7·MeCN**), $[Eu_2(phen)_2(pfb)_6]_n\cdot 4nMeOH$ (**7·MeOH**). Furthermore, on the example of compound $[Eu_2(phen)_2(1\text{-NAA})_2(pfb)_4]$ (**8**), it was shown that mixed-anionic compounds can be obtained by combining the more flexible 1-naphthaleneacetate (1-NAA) and pfb anions. In compounds **3** and **6**, some anion positions are disordered because both 1-nap and pfb anions occupy the same positions in varying ratios. The examples demonstrate that careful optimization of non-covalent interactions enables precise control over the structure and physicochemical properties of these coordination compounds, resulting in improved luminescent performance. The obtained compounds were characterized by single-crystal and powder X-ray diffraction, luminescence spectroscopy, infrared (IR) spectroscopy, and elemental (CHN) analysis. The photoluminescent properties were studied for the solid-state samples. Additionally, the density functional theory (DFT) method was employed to model the frontier molecular orbitals of the complexes and analyze their electronic structures.

Introduction

Photoluminescence represents an enthralling phenomenon that profoundly influences various aspects of modern society. Its versatility underpins numerous critical technologies from medical imaging and diagnostic tools to advanced energy solutions such as photocatalysis, solar cells, and cutting-edge optoelectronics.[1–4] Driven by the escalating demand for diverse photoluminescent materials, researchers across generations have relentlessly explored innovative approaches, leading to the development of a wide array of luminophores spanning from traditional molecular dyes to sophisticated luminescent nanostructures.[5–7]

Of particular interest among these innovations are luminescent lanthanide complexes, owing to their unique photophysical properties. The narrow bandwidth of the f–f transitions, the long luminescence lifetime (~ms), and the presence of high magnetic anisotropy determine the interest of the investigations carried out and the prospects for practical use.[8] Such distinctive features render lanthanide complexes invaluable both scientifically and commercially, enabling breakthroughs in fields including biomedical imaging, environmental sensing, renewable energy systems, security tagging *via* optical barcodes, and next-generation display technologies.[9–12]

The rational design of lanthanide ion's ligand environment is pivotal in shaping the structural architecture of coordination compounds, maximizing sensitization efficiency of lanthanide luminescence, and mitigating luminescence quenching

[a]*N. S. Kurnakov Institute of General and Inorganic Chemistry, Russian Academy of Sciences, Leninsky Prospect, 31, 119991 Moscow, Russian Federation. E-mail: shmelevma@yandex.ru*
[b]*N. D. Zelinsky Institute of Organic Chemistry, Russian Academy of Sciences, Leninsky Prospect., 47, 119991 Moscow, Russian Federation*
[c]*P. N. Lebedev Physical Institute of the Russian Academy of Sciences, Leninsky Prospect, 53, 119991 Moscow, Russian Federation*

processes.[13–16] Advancing targeted synthetic strategies toward lanthanide-based coordination compounds with optimized photoluminescent properties stands as a pressing challenge in modern coordination chemistry.

The current research works describe a variety of approaches aimed at enhancing the photoluminescent properties of lanthanide coordination compounds, which are generally focused on maximizing the absorption of radiation by the ligand environment of the lanthanide ion, the most efficient transfer of energy from the ligand environment to the lanthanide ion, and minimizing all possible pathways of its non-radiative loss. The most common approaches include: selection of the optimal ligand environment for efficient energy transfer to the metal ion, including utilizing of quantum chemistry methods;[17–20] reduction of the luminescence quenching effect by removing solvent molecules from the coordination sphere of lanthanide ions or employing fluorinated ligands to minimize quenching effect caused by vibrations in C–H bonds;[21–24] synthesis of heterometallic complexes composed of lanthanide – post-transition metal(d^{10}) such as Zn^{2+} or Cd^{2+} ions, which alter the triplet level energy of organic ligands and affects the efficiency of energy transfer to the lanthanide ion.[25–27] As well promising directions for enhancing the photoluminescent properties of europium compounds include: sensitization of Eu(III) PL through the organic ligand's singlet state,[28,29] sensitization of Eu(III) PL by thermally activated delayed fluorescence (TADF) emitters,[30] sensitization of Eu(III) PL by a metalloligand,[31,32] sensitization of Eu (III) PL by metallophilic stacks,[33,34] Yb-to-Eu cooperative sensitization.[35,36]

One particularly promising and least explored strategy lies in harnessing non-covalent interactions, notably intramolecular and intermolecular hydrogen bonding, π-stacking effects, and halogen-mediated interactions. By strategically engineering these interactions, precise control over the geometric arrangement and physicochemical attributes of the resulting complexes can be achieved.[37–40] Significantly, intentional engineering of diverse non-covalent interactions in lanthanide luminescent complexes profoundly boosts their luminescence efficiency by enabling highly effective energy transfer mechanisms across the entire conjugated system.

Herein, we report an efficacious route that entails the incorporation of predetermined sets of non-covalent interactions into compound architectures through the synthesis of mixed-anionic complexes incorporating several anions derived from aromatic monocarboxylic acids. The broad accessibility of aromatic carboxylates, combined with facile functionalization techniques, enables tailored assembly of non-covalent interaction networks, ensuring enhanced performance when diverse ligands are incorporated synergistically within a single framework.[41–45]

We have successfully synthesized a series of mixed-anionic complexes, highlighting the exceptional opportunities afforded by combining different types of anions. Expanding on previous research into benzoate-pentafluorobenzoate lanthanide systems, our findings reveal that incorporating a second type of anion substantially improves photoluminescence characteristics while concurrently modifying both the geometric arrangement of the central metal ion and the polyhedral structure of rare earth elements, as well as reconfiguring the broader non-covalent interaction framework compared to strictly monoanionic species.[41–43]

In this present study, we delved deeper into the exploration of mixed-anionic complexes featuring pentafluorobenzoate anions, further advancing our insights into the influence of substituent groups on both structural arrangements and optical behavior of these complexes. This work reports the synthesis of novel europium complexes comprising mixtures of 1-naphthoic or 1-naphthaleneacetic acid and pentafluorobenzoate anions, coupled with either 1,10-phenanthroline or 2,2′-bipyridine molecules, under variable ratios of the constituent anions. The use of these anions enables analysis of the structural dependence of mixed-carboxylate complexes on the size of the aromatic system within the anion. The presence of a CH_2-linker between the aromatic fragment and the carboxyl group in 1-naphthaleneacetic acid anions allows investigation of complexes containing conformationally flexible substituents. Detailed investigations of the crystallographic structures of these compounds were conducted, their photoluminescent properties thoroughly characterized, essential non-covalent interactions responsible for structure formation elucidated, and comparative analyses performed between the geometries of the mixed-anionic complexes and their corresponding homoanionic analogues.

Results and discussion

Synthesis of complexes and IR spectroscopy

The synthesis of complexes containing 1-naphthoate anions presents several challenges due to their inherently poor solubility, in contrast to pentafluorobenzoate complexes, which generally demonstrate excellent solubility profiles and simple preparatory procedures in both aqueous and organic media.

The formation of mixed-anionic 1-naphthoate-pentafluorobenzoate complexes is achievable, provided their thermodynamic favourability outweighs the tendency towards crystallization of less-soluble mono-anionic naphthoate derivatives. Our initial attempt involved preparing europium naphthoate by reacting europium sulfate with barium salts of 1-naphthoic acid in aqueous solution. Unfortunately, the precipitated product consisted of both poorly soluble europium naphthoate and insoluble barium sulfate, compounded by the inability to recrystallize the resultant 1-naphthoic acid salt due to insufficient solubility in accessible organic solvents. Consequently, we opted for a reaction between europium pentafluorobenzoate $[Eu_2(H_2O)_8(pfb)_6]$ and 1-naphthoic acid under varying stoichiometric conditions, yielding a series of novel 1-naphthoate-pentafluorobenzoate europium complexes with distinct compositions (see Scheme 1).

Treatment of europium pentafluorobenzoate $[Eu_2(H_2O)_8(pfb)_6]$ with five equivalents of 1-naphthoic acid in

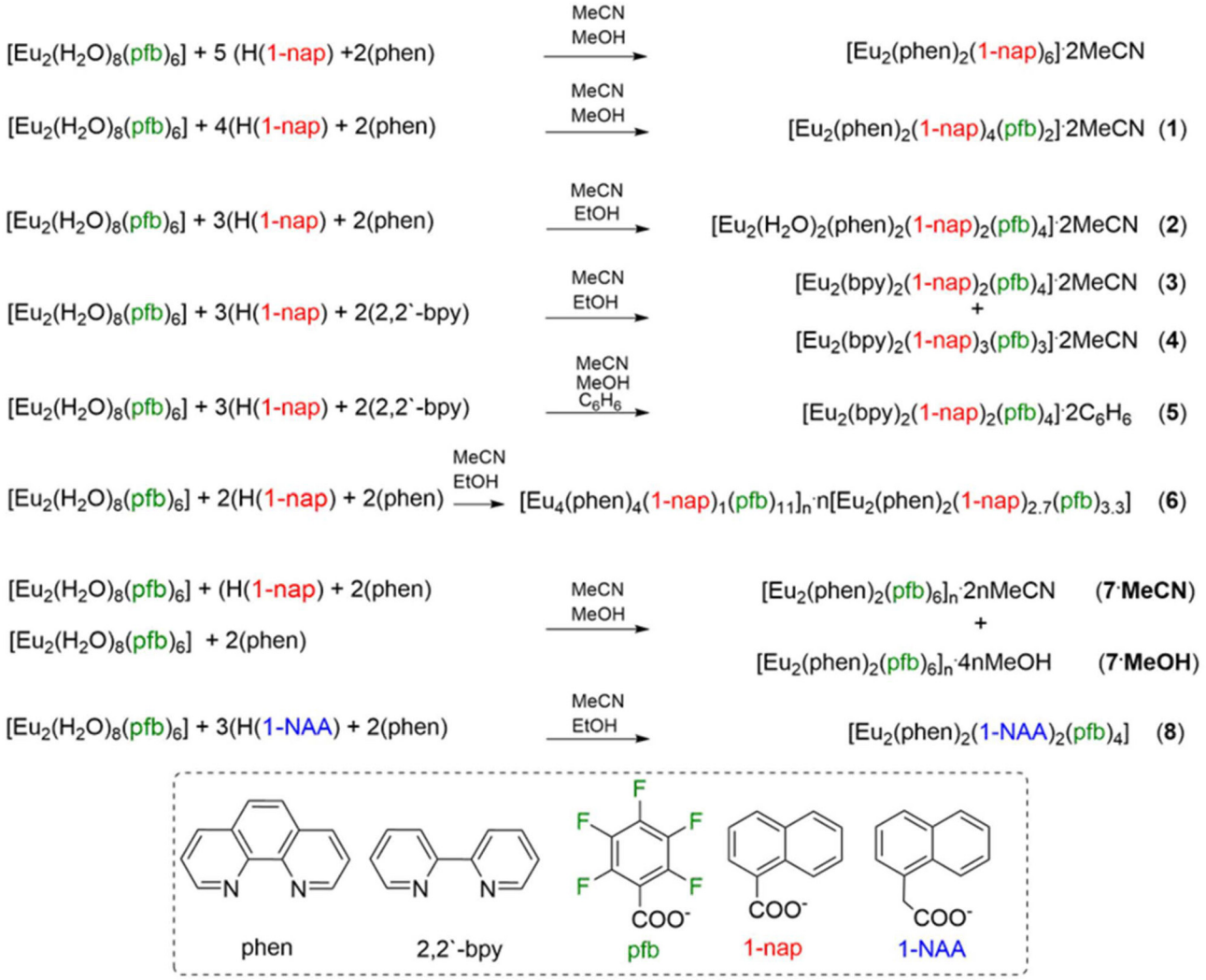

Scheme 1 Synthesis of compounds **1–8**.

the presence of 1,10-phenanthroline (phen) resulted in the complete displacement of all pentafluorobenzoate anions, yielding exclusively the previously reported, sparsely soluble homoanionic naphthoate complex $[Eu_2(phen)_2(1\text{-}nap)_6]$ (Scheme 1).[46] Even a slight deficiency of one equivalent of 1-naphthoic acid did not prevent the full replacement of pentafluorobenzoate anions. Using four equivalents of 1-naphthoic acid yielded a mixed-anionic complex $[Eu_2(phen)_2(1\text{-}nap)_4(pfb)_2]\cdot 2MeCN$ (**1**, Scheme 1), containing exactly four 1-naphthoate and two pentafluorobenzoate anions according to the applied stoichiometry. This complex was obtained in a phase-pure form and rigorously evaluated concerning its photoluminescent properties (Fig. S1).

Further decreasing the quantity of 1-naphthoic acid to three equivalents led to the formation of a mixed-anionic compound $[Eu_2(H_2O)_2(phen)_2(1\text{-}nap)_2(pfb)_4]\cdot 2MeCN$ (**2**, Scheme 1), wherein each europium ion coordinates two pentafluorobenzoate (pfb) anions and one 1-naphthoate (1-nap) anion. Single-crystal X-ray diffraction analysis showed that the reaction mixture contained individual crystals of compound **1**. Hence, isolating compound **2** in sufficient purity for thorough photoluminescence characterization remains unrealized.

A prolonged crystallization for compounds **1** and **2** (about 45 days) is associated with the necessity of obtaining high-quality single crystals suitable for X-ray structural analysis. In contrast, faster evaporation of reaction mixture 1 over one week resulted in the formation of polycrystalline precipitate, which also corresponded to complex **1** according to powder X-ray diffraction data (XRD).

Replacing 1,10-phenanthroline with 2,2′-bipyridine (2,2′-bpy) under an analogous reagent ratio ($[Eu_2(H_2O)_8(pfb)_6]$: H(1-nap)) afforded crystals of $[Eu_2(2,2'\text{-}bpy)_2(1\text{-}nap)_2(pfb)_4]\cdot 2MeCN$ (**3**, Scheme 1). The phase purity of compound **3** was confirmed by XRD analysis (Fig. S2). Subsequent slow evaporation of the residual solution following isolation of compound **3** afforded crystals of two distinct compositions: compound **3** and $[Eu_2(2,2'\text{-}bpy)_2(1\text{-}nap)_3(pfb)_3]\cdot 2MeCN$ (**4**, Scheme 1). The latter exhibits partial occupancy of two positions by a random

mixture of pentafluorobenzoate and 1-naphthoate anions in a 0.5/0.5 ratio, indicating positional disorder. Thus, the crystal appears to contain a mixture of configurations with approximate compositions $[Eu_2(2,2'\text{-bpy})_2(1\text{-nap})_2(pfb)_4]$ and $[Eu_2(2,2'\text{-bpy})_2(1\text{-nap})_4(pfb)_2]$ in equal proportion. Executing a similar reaction in an acetonitrile-benzene solvent mixture rather than pure acetonitrile yielded compound $[Eu_2(2,2'\text{-bpy})_2(1\text{-nap})_2(pfb)_4]\cdot 2C_6H_6$ (**5**, Scheme 1), which crystallizes as a benzene solvate. The phase purity of this compound was confirmed by XRD measurements (Fig. S3).

Reduction of H(1-nap) to two equivalents in the reaction with europium pentafluorobenzoate $[Eu_2(H_2O)_8(pfb)_6]$ and 1,10-phenanthroline afforded an unusual cocrystal $[Eu_4(phen)_4(1\text{-nap})_1(pfb)_{11}]\cdot n[Eu_2(phen)_2(1\text{-nap})_{2.7}(pfb)_{3.3}]$ (**6**, Scheme 1). This cocrystal consists of a coordination polymer $[Eu_4(phen)_4(pfb)_{11}(1\text{-nap})]_n$ and a binuclear mixed-carboxylate complex $[Eu_2(phen)_2(1\text{-nap})_{2.7}(pfb)_{3.3}]$, with one molecule of the binuclear complex per tetranuclear unit of the polymeric chain.

Within the structure of both the polymer chain and the binuclear complex, two anion positions are refined as mixtures of pfb and 1-nap anions with occupancies of 0.5/0.5 and 0.65/0.35, respectively. Although crystals of compound **6** reproduced with preserved occupancy ratios of pfb/1-nap anions, obtaining phase-pure material remains challenging. Powder X-ray diffraction reveals the presence of additional polycrystalline phases whose identities cannot yet be determined. Probably, slower evaporation of the reaction mixture combined with continuous removal of formed precipitates or variations in solvents used for synthesis and crystallization, may allow selecting optimal conditions for isolating compound **6** as a phase-pure product.

Further decreasing the amount of 1-naphthoic acid to one equivalent led to the crystallization of a mixture of pentafluorobenzoate coordination polymers: $[Eu_2(phen)_2(pfb)_6]_n\cdot 2n$MeCN (**7·MeCN**, Scheme 1) and $[Eu_2(phen)_2(pfb)_6]_n\cdot 4n$MeOH (**7·MeOH**, Scheme 1), which differ in structure. These polymers were also obtained by reacting $[Eu_2(H_2O)_8(pfb)_6]$ with two equivalents of phen. Experimental details describe the methodology for obtaining crystals **7·MeCN** and **7·MeOH** without adding any 1-naphthoic acid.

Additionally, under similar experimental conditions, a mixed-anionic complex incorporating 1-naphthaleneacetic acid (1-NAA) and pentafluorobenzoic acid anions was synthesized (Scheme 1). The presence of a CH_2-linker between the carboxyl group and the aromatic moiety provides greater conformational flexibility, allowing for comparison of non-covalent interactions between pentafluorophenyl and naphthyl fragments in different systems. Reaction of europium pentafluorobenzoate $[Eu_2(H_2O)_8(pfb)_6]$ with three equivalents of 1-naphthaleneacetic acid and 1,10-phenanthroline yields the mixed-anionic compound $[Eu_2(phen)_2(1\text{-NAA})_2(pfb)_4]$ (**8**, Scheme 1).

The observed disproportionate increase in the pentafluorobenzoate anion presence in compounds **2** and **6** appears to be natural because the solubility of the resulting compounds constantly increases as the number of 1-naphthoate anions in the compounds decreases. Consequently, the efficiency of protonation by the weaker 1-naphthoic acid on the stronger pentafluorobenzoic acid anions diminishes. This phenomenon results in only being able to isolate crystals of the compound **7**, even when introducing just one equivalent of 1-naphthoic acid.

The IR spectra of the synthesized compounds were acquired within a spectral range from 4000 to 550 cm^{-1}. All compounds display broad, low-intensity bands between 3200 and 3000 cm^{-1}, attributable to stretching vibrations of hydrogen-bonded C–H moieties associated with aromatic rings of the acid ligands. Within the interval of 1630–1360 cm^{-1}, multiple intense absorption peaks arise, which correspond to both asymmetric and symmetric stretching modes of carboxylic acid groups. The notable red-shifted nature of these frequencies when compared to isolated free acids provides strong evidence for the formation of coordination complexes by means of ligand–metal interactions mediated through the respective functionalities.

Additionally, in the range of 1370–1523 cm^{-1}, various features emerge, including C–H vibrations originating from the phenanthroline ring systems, as well as contributions from acetonitrile (MeCN) solvent molecules where applicable. Further, in the region spanning 1340–1420 cm^{-1}, additional absorptions related to carbon–carbon double bond stretches within the aromatic cycles of phenanthroline-based derivatives and carbonyl groups belonging to naphthoate or other carboxylate-type ligands become evident. Lastly, weaker absorbances around 1000 cm^{-1} may indicate C–F stretching vibrations within perfluorobenzene components while broader regions centered at approximately 720–900 cm^{-1} reflect out-of-plane bending modes linked to the aromatic frameworks of both phenanthroline and naphthalene-derived entities (or naphtoic acid anion).

Gas-phase density functional theory (DFT) calculations reproduce well the molecular structures and interatomic distances ascertained *via* X-ray crystallography (Table S6). Detailed comparisons of specific bond lengths and valence angles corroborate these findings. Furthermore, the calculated infrared (IR) spectra demonstrate exceptional congruence with the experimental IR data acquired using attenuated total reflectance (ATR) spectroscopy for compounds **1–8**. This methodology enables both a transparent delineation of ligand contributions within discrete spectral regions and an exact determination of frequency shifts accompanying metal–ligand coordination events.

The structure of complexes

Complexes **1–5** are binuclear systems in which europium ions, connected by bridging and chelating–bridging carboxylate anions, coordinate to chelating 1,10-phenanthroline or 2,2′-bipyridine ligands (Fig. 1 and Table 1). In all cases, the nine-coordinate polyhedra of Eu^{3+} have the "muffin" geometry (EuO_7N_2, Table S3), consisting of two nitrogen atoms from the phen or 2,2′-bpy ligands and seven oxygen atoms from two

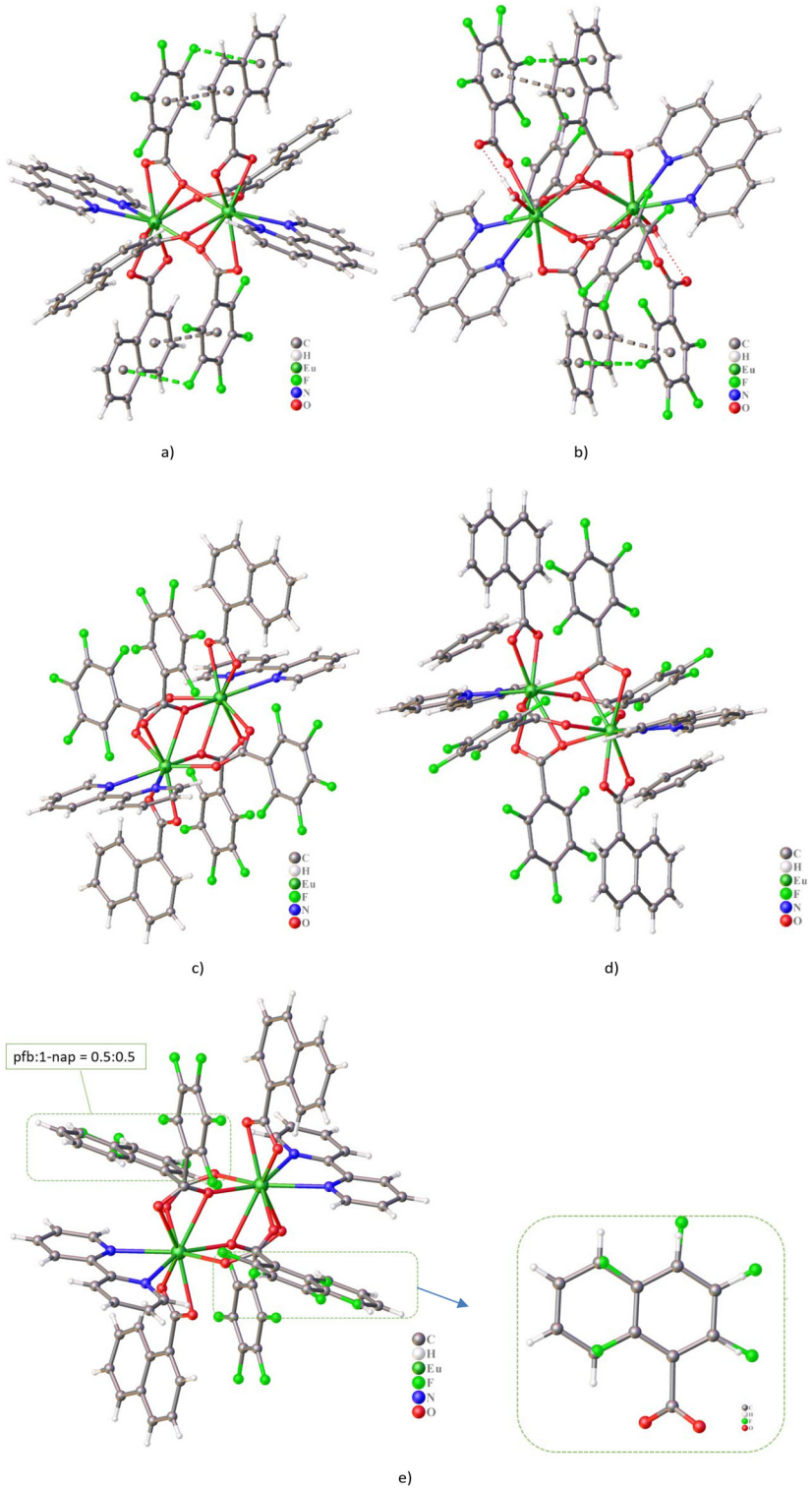

Fig. 1 Structure of complexes **1** (a), **2** (b), **3**(c), **5**(d), and **4**(e). Solvate molecules are omitted for clarity. Dashed lines indicate π···π and C–F···π interactions, as well as hydrogen bonds. In panel (e), dashed lines highlight parts of the molecules where anion positions are disordered.

bridging anions, two chelating–bridging anions, and one chelating–bridging anion coordinated to a metal center through monodentate coordination of its oxygen atom.

In complex **2**, an additional water molecule coordinates to the metal ion and, as a result, one anion coordinates in a monodentate fashion while the uncoordinated oxygen atom of

Table 1 Basic geometric parameters of the complexes **1–5**

	d, Å				
Bond	**1**	**2**	**3**	**4**	**5**
Eu–N	2.570(4), 2.623(4)	2.567(9)–2.637(8)	2.566(5), 2.607(5)	2.569(5), 2.575(4)	2.582(6), 2.584(5)
Eu–O (1-nap)	2.351(3)–2.441(3)	2.294(7)–2.798(8)	2.416(5), 2.457(5)	2.423(4), 2.451(4)	2.415(4), 2.424(5)
Eu–O (pfb)	2.390(3)–2.605(3)	2.383(7)–2.434(7)	2.380(5)–2.576(5)	2.372(4)–2.586(4)	2.367(4)–2.624(4)
Eu–O (pfb/1-nap)	—	—	—	2.384(4), 2.391(4)	—
Eu–O (H_2O)	—	2.387(7), 2.395(7)	—	—	—
Eu···Eu	4.015(1)	4.094(1)	3.995(1)	4.029(1)	4.037(1)
Angle	***ω*, °**				
Main plane···N-donor	106.9(1)	99.5(3) 103.3(3)	104.6(2)	92.7(2)	92.4(2)
Main plane···pfb equator	95.7(1)	59.3(3)	103.3(3)	80.7(2)	102.0(1)
Main plane···nap equator	87.48(7)	51.5(2)	92.9(2)	85.6(1)	96.2(1)
pfb···1-nap	4.4(2)	5.4(4)	11.7(3)	2.8(4)	9.9(2)
Main plane···COO^- bridge	83.56(8)	87.9(2) 88.2(2)	83.5(1)	89.0(1)	91.1(1)
Ar(bridge)···COO^- bridge	30.1(2)	41.8(4) 46.5(4)	50.8(3)	49.0(2)	48.6(3)

the carboxylate group forms a classical hydrogen bond with the water molecule (Fig. 1b and Table S4). In the equatorial regions of complexes **1**, **2**, and **5**, intramolecular C–F···π interactions occur between a fluorine atom of the pfb anion and the aromatic fragment of a 1-nap anion. Additional π···π stacking is observed between pfb and 1-nap fragments. By contrast, in complexes **3** and **4**, the distances between the analogous aromatic fragments exceed 4 Å (Fig. 1 and Tables 2 and S5).

Table 2 Table of π···π interactions in crystal packing of complexes **1**, **2**, **5–8**

Interactions	Cg···Cg, Å	Cg···Perp, Å	Symmetry code	*α*, °
Complex **1**				
phen···1-nap	3.644(3)	3.323(2)	$3/2-x,1/2+y,z$	6.5(3)
1-nap···pfb	3.581(3)	3.283(2)	$1-x,1-y,1-z$	4.3(2)
phen···phen	3.583(4)	3.442(3)	$2-x,1-y,1-z$	0.0(3)
Complex **2**				
phen···phen	3.722(6)	3.658(4)	$1-x,-1/2+y,1-z$	15.2(5)
1-nap···pfb	3.685(7)	3.449(5)		3.8(6)
1-nap···pfb	3.704(7)	3.469(5)		6.9(6)
Complex **5**				
1-nap···pfb	3.779(4)	3.383(3)		9.5(3)
Complex **6**				
pfb···phen	3.616(9)	3.597(4)		14.1(7)
pfb···pfb	3.659(4)	3.410(4)	$1-x,-y,-z$	7.2(4)
1-nap···phen	3.437(4)	3.358(3)	$1-x,-y,-z$	8.7(3)
phen···phen	3.658(11)	3.532(4)		1.6(9)
phen···phen	3.522(13)	3.515(10)		2.2(8)
1-nap···pfb	3.751(3)	3.465(3)		3.7(3)
Complex **7·MeCN**				
phen···phen	3.729(5)	3.650(3)		12.8(4)
pfb···pfb	3.444(5)	3.427(4)		5.8(4)
pfb···pfb	3.589(5)	3.315(3)		11.6(4)
Complex **7·MeOH**				
phen···pfb	3.799(5)	3.379(3)	$1-x,2-y,1-z$	20.6(4)
phen···pfb	3.592(5)	3.536(3)		11.8(4)
Complex **8**				
phen···phen	3.606(10)	3.434(7)	$1-x,2-y,-z$	1.8(8)
pfb···pfb	3.465(15)	3.440(10)	$-x,1-y,-z$	5.0(9)
pfb···pfb	3.408(16)	3.311(11)	$-x,1-y,-z$	0

In the molecules of compounds **1–5**, a principal plane can be distinguished, formed by the metal ions and the carboxylate groups of the chelating–bridging anions, while the planes formed by the bridging carbonyl groups with the metal ions above and below the central plane are nearly perpendicular to it. The planar N-donor ligands are arranged analogously to the bridging anions but rotated by about 100° relative to the central plane (Table 1). Thus, the metal–oxygen framework of complexes **1–5** is largely conserved, regardless of the nature of the N-donor ligand or the anionic ratio.

Since all complexes **1–5** are mixed-anion systems, it is important to analyze the positions of the anions within the molecules and their orientation relative to the principal plane of the molecule. In complexes **1**, **3–5**, pentafluorobenzoate anions act as chelating–bridging ligands, whereas 1-naphthoate serves as the chelating ligand. In complex **2**, the roles are reversed: the sterically larger 1-naphthoate becomes chelating–bridging due to the presence of a coordinating water molecule, while the more compact pentafluorobenzoate occupies a single coordination site. In all complexes, the 1-naphthoate anions have nearly planar conformations. The pentafluorobenzoates in complexes **1**, **3–5** exhibit carboxylate groups oriented nearly perpendicular to the aromatic ring (Table 1), with their aromatic fragments almost orthogonal to the principal plane. In complex **2**, by contrast, the pfb anion becomes planar due to hydrogen-bond formation, whereas the naphthoate ring system rotates by 40(2)°, placing the fused rings at 50–60° relative to the principal plane (Table 1).

The nearly perfectly parallel arrangement of the aromatic fragments is facilitated by the formation of intramolecular π···π interactions (Table 2). Above and below the main molecular plane lie the bridging anions, whose carboxylate groups are nearly perpendicular to it. Notably, the bridging function is performed by the predominant anion type: in complexes **1**, **3**, and **5** by pfb, in complex **2** by nap, and in complex **4** by both anions in a 0.58/0.42 ratio. This is reflected in crystallographic disorder, as revealed by single-crystal X-ray data, where two

aromatic fragments share the same position with the corresponding occupancies. The aromatic rings of bridging anions are rotated 30–50° relative to their carboxyl groups in all cases, owing to intermolecular π···π stacking with neighboring molecules and additional interactions with solvent molecules – benzene in complex **5** or acetonitrile in complexes **2–4** (Tables 1 and 2). In complex **1**, acetonitrile solvate molecules interact through weak C–H···O, C–H···F, and C–H···N contacts (Tables S4 and S5).

It was found that the incorporation of a second type of anion into complex **1** affects both the geometric positions of the anionic substituents and the geometry of the metal core, compared to the mono-anionic naphthoate complex $[Eu_2(phen)_2(1\text{-nap})_6]$.[26] In particular, the Eu···Eu distance is shortened by 0.15 Å in complex **1**, while Eu–N and Eu–O bond lengths differ by no more than 0.1 Å. In complex **5**, intramolecular π···π interactions occur between pfb and 1-nap anions.

The packing of molecules **1–5** in the crystals is mainly stabilized by π···π interactions and forms a three-dimensional network, with solvent molecules localized within its cavities (Fig. 2 and Table 2). The only exception is complex **2**, in which the primary molecular synthon consists of hydrogen-bonded chains (Fig. 3 and Table S4) interconnected by π···π interactions and interactions between acetonitrile molecules and pentafluorobenzoate rings. In **2**, this is close to a classical LP-H···π interaction, with the shortest distance from the nitrogen atom of acetonitrile to the ring carbon of 3.41(2) Å and a C–N···Cg angle of 126(1)°. In the crystals of **3** and **4**, the interaction is closer to the π···π type, with N···Cg distances of 3.29(2) Å and 3.484(13) Å, and C–N···Cg angles of −116.3(2)° and 85.7(9)° in **3** and **4**, respectively. Multiple C–F···π, C–H···O, and C–H···F interactions are also involved in stabilizing the crystal packing of complexes **1–5** (Tables S4 and S5).

Compound **6** crystallizes as a cocrystal composed of a polymeric chain $[Eu_4(phen)_4(1\text{-nap})_1(pfb)_{11}]_n$ and a binuclear molecule $[Eu_2(phen)_2(1\text{-nap})_{2.7}(pfb)_{3.3}]$ (Fig. 4). Both complexes are mixed-anion systems: in the molecular complex, the 1-nap anion is chelating, the pfb anion serves a bridging function, and the chelating–bridging positions are occupied by 1-nap/pfb with equal probability (Table 3). The polymeric chain consists of binuclear units in which the rare-earth element ions, coordinated by chelating phenanthroline molecules, are linked by four bridging anions, two of which are stably occupied by pfb anions and the other two may be occupied by either pfb or 1-nap anions with a probability of 0.65/0.35. Each europium ion coordinates a phen molecule to complete its coordination environment as a square antiprism (EuO_7N_2, Table S3). The units are connected *via* two bridging pfb anions, leading to π···π interactions between phen molecules of adjacent units (Table 2). It is important that, although

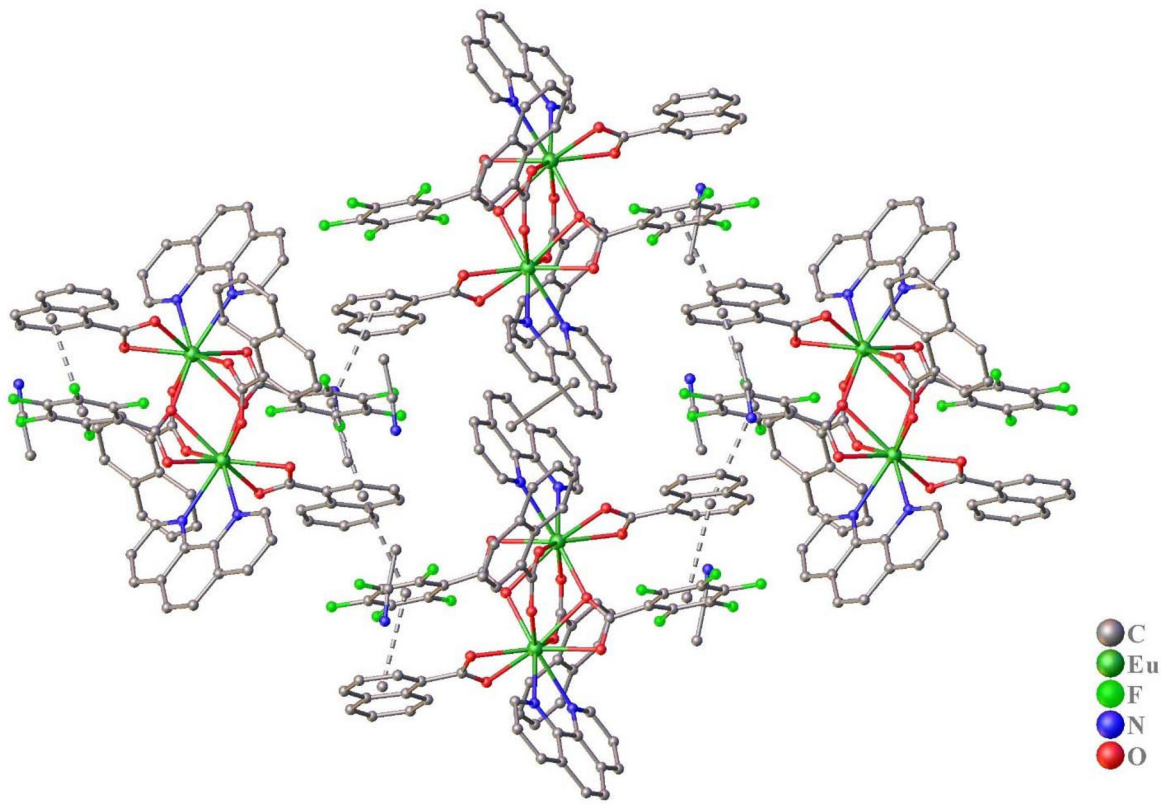

Fig. 2 π···π interactions in the crystal structure of compound **1**. Hydrogen atoms are omitted for clarity.

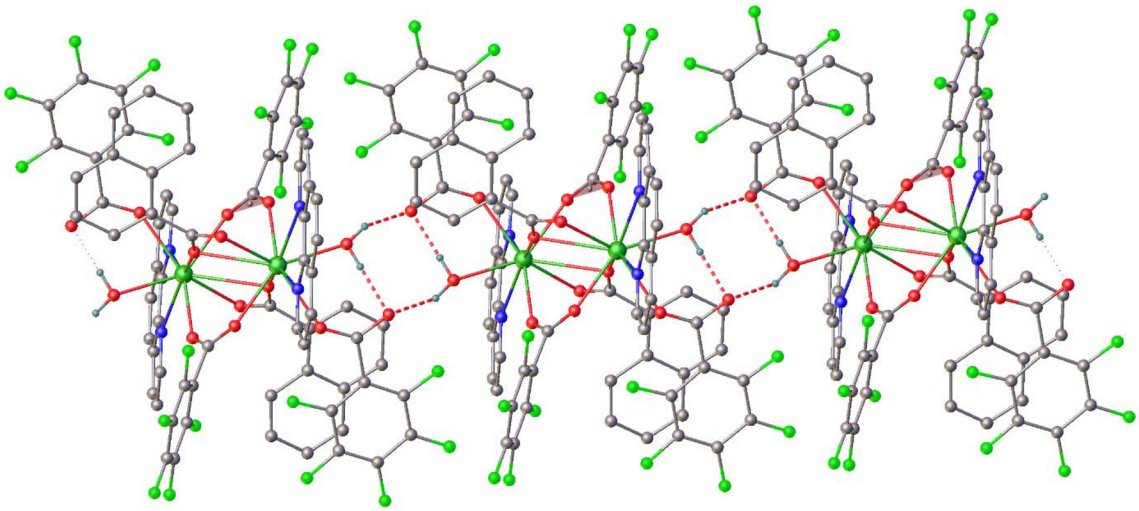

Fig. 3 Infinite hydrogen-bonded chain in crystals of compound **2**. Hydrogen atoms of carbon are omitted for clarity.

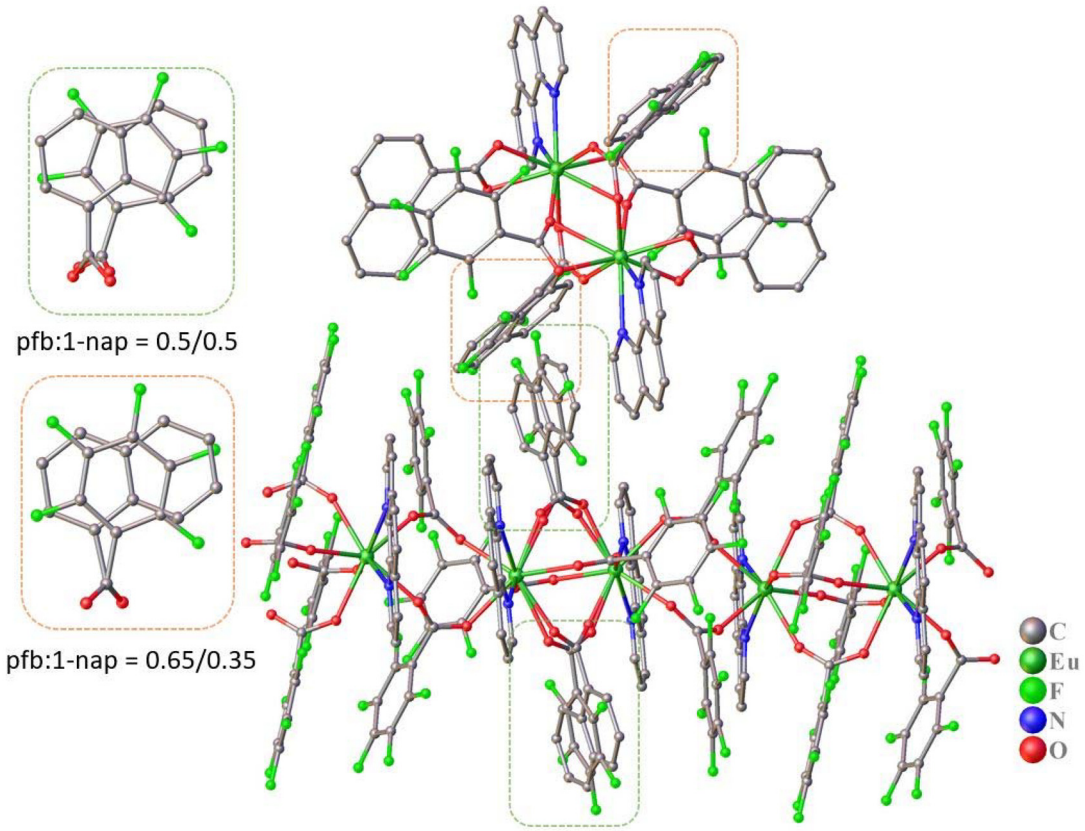

Fig. 4 Fragment of the crystal packing of compound **6**. Dashed lines indicate molecular fragments with disordered anion positions. Hydrogen atoms are omitted for clarity.

one of the phenanthroline fragments is completely disordered, the interacting fragments are arranged almost perfectly parallel to each other, with the six-membered rings offset to maximize overlap.

In the binuclear molecule of compound **6**, a π···π interaction is formed between the 1-nap and pfb fragments. Crystal formation occurs through stacking interactions involving the aromatic systems of phen and pfb of the polymeric chain and

Table 3 Basic geometric parameters of the complexes **6–8**

	d, Å			
Bond	**6**	**7·MeCN**	**7·MeOH**	**8**
Eu–N (phen)	2.564(4), 2.598(4) $(Eu)_2$ 2.544(18)–2.627(5) $[Eu]_n$	2.556(7)–2.590(7)	2.577(8), 2.607(8)	2.546(11), 2.581(9)
Eu–O (1-nap)	2.436(4), 2.455(4) $(Eu)_2$	—	—	—
Eu–O (pfb)	2.383(6)–2.664(4) $(Eu)_2$ 2.333(4)–2.427(3) $[Eu]_n$	2.338(5)–2.437(5)	2.348(5)–2.431(6)	2.361(9)–2.437(11)
Eu–O (pfb/1-nap)	2.385(3), 2.388(3) $(Eu)_2$ 2.24(3)–2.49(3) $[Eu]_n$	—	—	—
Eu–O (1-NAA)	—	—	—	2.419(8), 2.549(8)
Eu–O (H_2O)	—	—	—	—
Eu···Eu	4.026(1) $(Eu)_2$ 4.448(1), 5.354(1) $[Eu]_n$	4.548(1), 5.427(1)	4.385(2), 6.020(2)	3.943(1)

the phen fragments of the molecular complex, which intercalate into the stack (Table 2). Further stabilization of the three-dimensional structure is provided by numerous C–H···O, C–H···F, C–H···π, and C–F···π interactions (Tables S4 and S5).

Complex **7·MeCN** (Fig. 5a and Table 3) has a structure analogous to the polymeric chain in compound **6**, with minimal differences in the geometry of the metal core. However, differences in the structure of the second component of the crystals lead to changes in the orientation of the aromatic ligand fragments. In compound **6**, the aromatic fragments of two phen molecules and one pfb anion, which participate in the formation of stacking interactions, are arranged almost parallel to each other and to the phen molecule of a neighboring binuclear complex intercalating into the π···π system, resulting in disruption of the aromatic stack order at this junction. In the crystal of **7·MeCN**, the acetonitrile molecule forms an N···π interaction (distance from the nitrogen atom to the ring carbon 3.041 Å), "pushing apart" the aromatic fragments of the pfb anions. The π···π system within the polymeric chains is sufficiently dense to prevent interpenetration of aromatic fragments and the formation of intermolecular stacking interactions.

The structure of the polymeric chain in complex **7·MeOH** differs from that in **7·MeCN** because two anions within the binuclear unit of the polymeric chain act as chelating–bridging ligands, resulting in a shortening of the Eu···Eu distances (Fig. 5b and Table 3). The aromatic ligand fragments in this complex are oriented such that infinite chains of stacking interactions are formed on both sides of the metal core, making the molecule more compact and leading to a reduction of the Eu···Eu distances not only within the main binuclear unit but also in the region of their connectivity (Table 2). The methanol solvate molecules are localized between stacks of aromatic fragments through classical O–H···O hydrogen bonds, both among themselves and with the oxygen atom of the coordinated anion (Table S4).

The metal core structure of complex **8** is analogous to the binuclear compounds **1–5** described above, with pentafluorobenzoate anions serving as bridging and bidentate ligands, while the more flexible 1-naphthoate anions act as chelating–bridging ligands (Fig. 6a and Table 3). Presumably due to their flexibility, the system of intramolecular π···π interactions between the aromatic fragments of the chelating–bridging and chelating ligands is disrupted. Instead, the pentafluorobenzene rings form weak intramolecular C–F···π interactions with the phenanthroline molecule and strong π···π interactions with an equivalent ring of a neighboring molecule (Fig. 6b and Tables 2, S5).

This interaction is further stabilized by T-stacking between the pentafluorobenzoate fragment and the phenanthroline molecule. As a result of these interactions, zigzag chains are formed, connected into a three-dimensional structure *via* π···π interactions between the pentafluorobenzene ring of the bridging anion and the naphthyl fragments of molecules from an adjacent chain.

Luminescent properties of complexes

The photoluminescent properties of the europium compounds **1**, **3**, and **5** containing 1-napthoate anions in the solid state were analyzed in detail. Upon ligand excitation, the compounds show typical narrow emission bands at 570–710 nm wavelength range, assigned to transitions from the excited $^5D_0$ state to the ground $^7F_{0-4}$ states of Eu^{3+} ion. Besides, the weak bands of $^5D_1 \rightarrow {}^7F_J$ (J = 0–2) transition of Eu^{3+} are observed in the 520–570 nm wavelength range. The emission spectra at 77 K and 300 K temperatures and λ_{ex} = 320 nm are shown in Fig. 7 and S4, respectively. The $^5D_0 \rightarrow {}^7F_0$ transition is a useful indicator of non-equivalent surrounding for Eu^{3+} ion, since the initial and final states are non-degenerate.[47] In the photoluminescence spectra of the investigated compounds, the corresponding transition is presented by a single symmetrical band indicating a one site for europium ion that is according with X-ray data. The energy of the $^5D_0 \rightarrow {}^7F_0$ transition is 17 232, 17 230, and 17 235 cm^{-1} for **1**, **3**, and **5**, respectively. Close value of the transition point to similar covalency of bonds between the Eu^{3+} ion and donor atoms of coordinated ligands. Nevertheless, the splitting pattern of the J levels indicates the differences in site symmetry. The $^5D_0 \rightarrow {}^7F_J$ (J = 0, 1, 2, 4) transitions of complex **1** display 1, 3, 5 and at least 8 com-

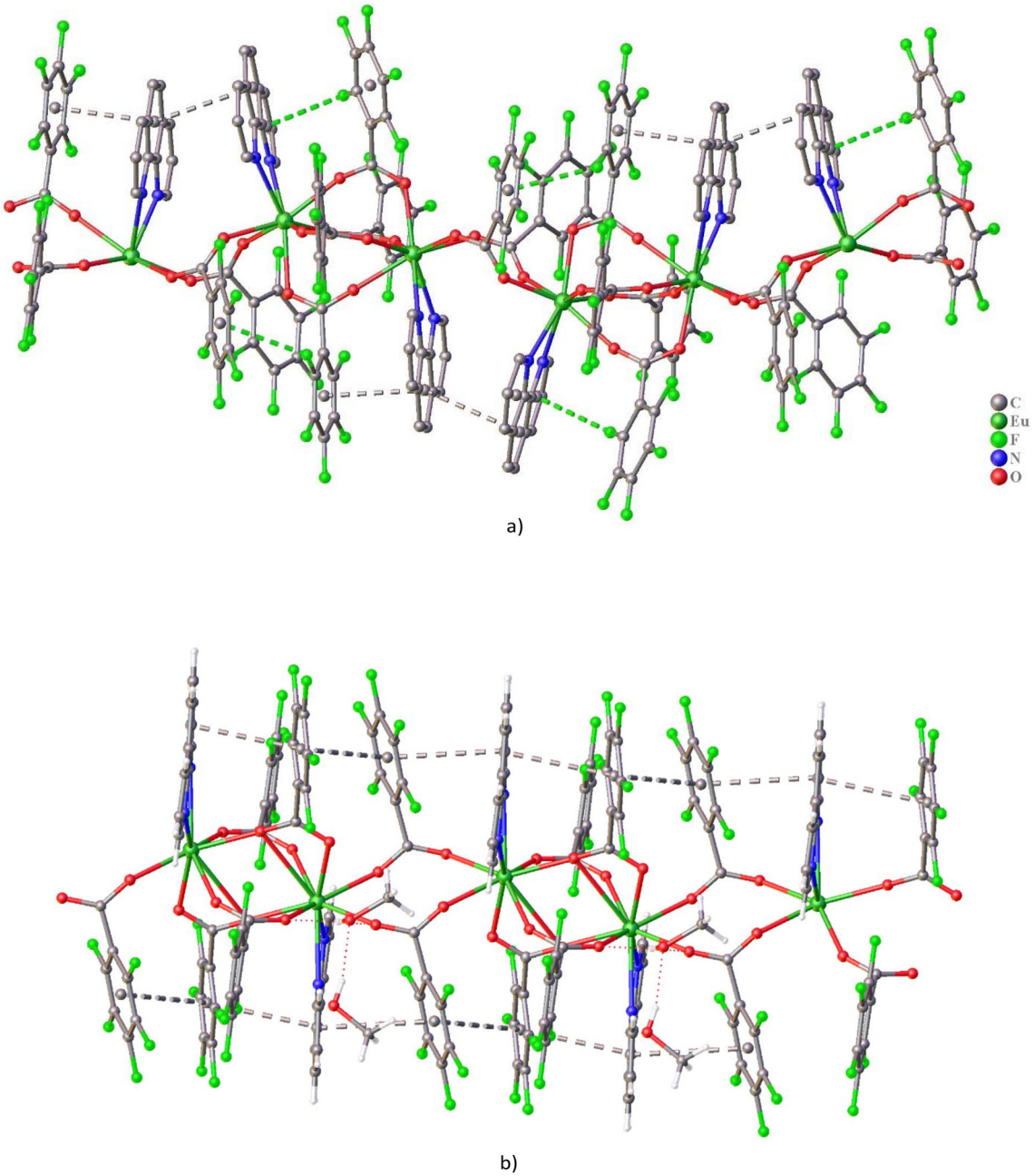

Fig. 5 Fragment of the polymeric chains of compounds **7·MeCN** (a) and **7·MeOH** (b). Dashed lines indicate π···π and C–F···π.

ponents that correlate with C_s symmetry of Eu^{3+} environment obtained by X-ray analysis. The 1, 2, 4 and 7 crystal-fields components of $^5D_0 \rightarrow {}^7F_J$ (J = 0, 1, 2, 4) transitions, respectively, observed for complexes **3** and **5**, are in a good agreement with C_{4v} symmetry.

The higher symmetry observed for compounds **3** and **5** may be attributed to the reduced steric hindrance of 2,2′-bipyridine compared to 1,10-phenantroline, due to the higher flexibility of the first one.[48] The ratio of the integral intensity of the induced electric dipole transition $^5D_0 \rightarrow {}^7F_2$ to the magnetic dipole transition $^5D_0 \rightarrow {}^7F_1$ of complex **1** is 8.15, which indicates a strong deviation of the Eu^{3+} environment from inversion symmetry,[48] whereas the intensity ratios $^5D_0 \rightarrow {}^7F_2/{}^5D_0 \rightarrow {}^7F_1$ for complexes **3** and **5** are lower, at 5.87 and 5.59, respectively.

In addition to the line-like luminescence of the europium ion, a weak broad band in the 360–550 nm wavelength range is observed in the emission spectra of complexes **3** and **5** (Fig. S5). This emission can be attributed to ligand-centered luminescence. Despite the low intensity of the band, its presence indicates an ineffective energy transfer from the ligand environment to the europium ion.

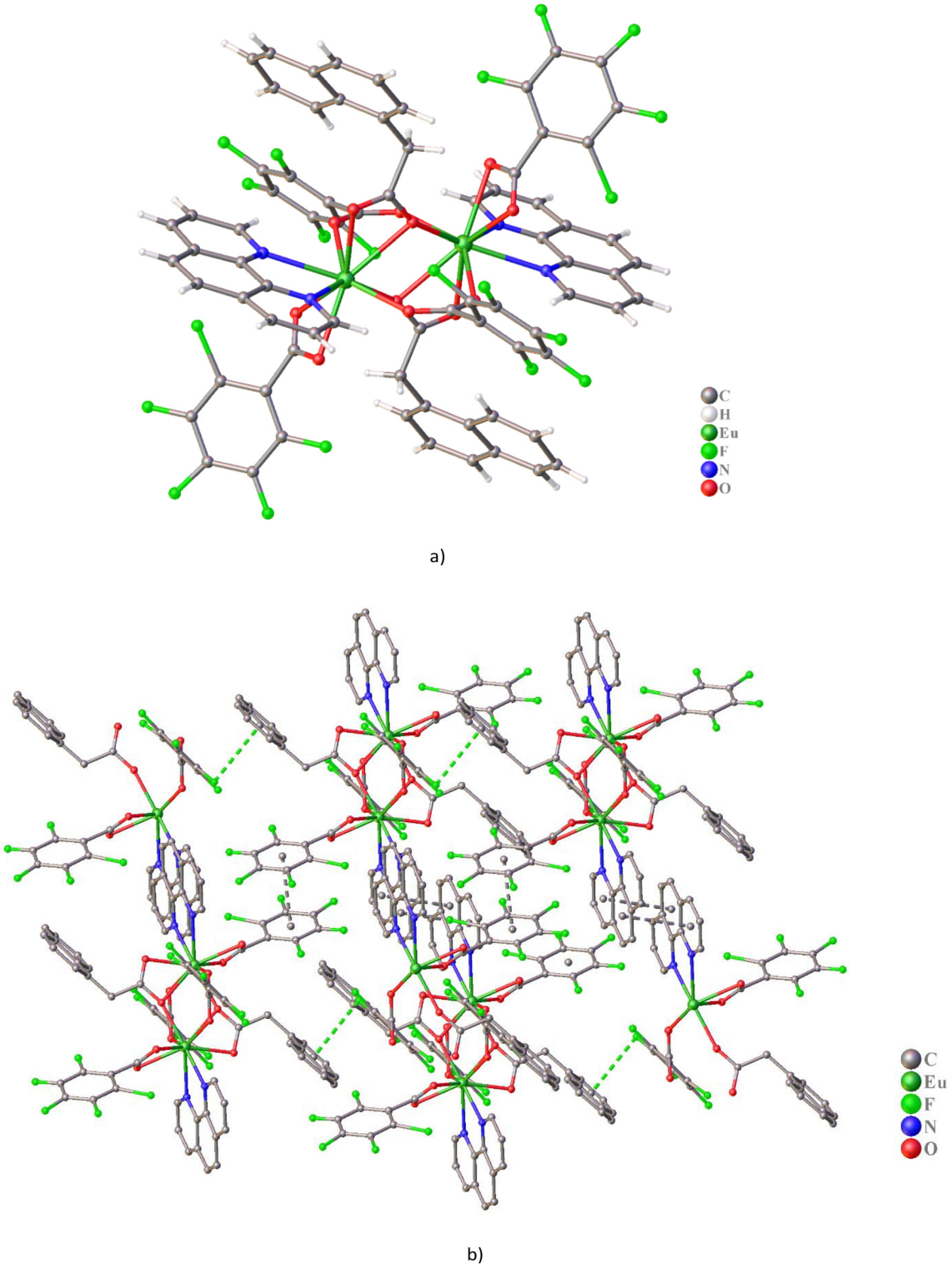

Fig. 6 Crystal structure (a) and a fragment of the crystal packing (b) of compound **8**. In (b), hydrogen atoms are omitted for clarity. Dashed lines indicate π···π and C–F···π interactions.

Excitation spectra of complexes **1**, **3** and **5** were recorded for the most intense $^5D_0 \rightarrow {}^7F_2$ transition of Eu^{3+} (Fig. 8 and S6). In addition to the narrow f–f transition of europium ion, the spectra demonstrate intense broad π–π* ligand absorption bands, with long-wavelength maxima at about 350 nm for complex **1** and about 325 nm for complexes **3** and **5**, indicating the effective energy transfer from the ligand environment to the europium ion. The long-wavelength maxima are attributed

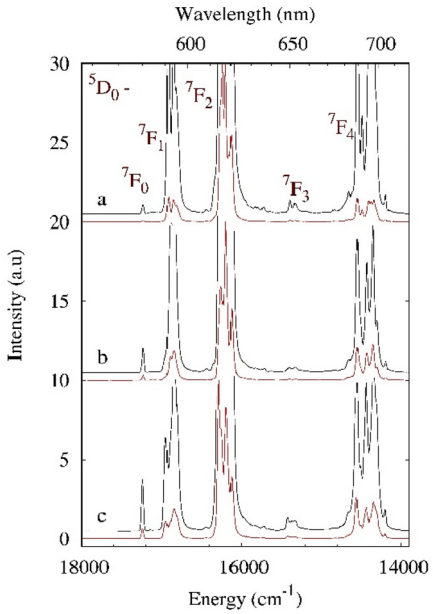

Fig. 7 Luminescence spectra of **1** (a), **3** (b) and **5** (c) at 77 K, λ_{ex} = 320 nm. The black line indicates the spectra at an enlarged scale.

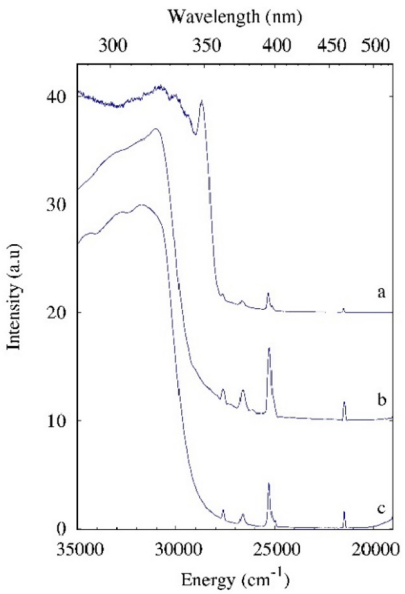

Fig. 8 Excitation spectra of **1** (a), (b) and **5** (c) at 77 K, λ_{em} = 615 nm.

to n, $\pi \rightarrow \pi^*$ transitions of the 1,10-phenantroline in complex **1** and 2,2′-bipyridine in complexes **3** and **5**. Furthermore, the weak shoulder observed in the 340–400 nm region of the excitation spectra of complexes **3** and **5** and can be assigned to a charge transfer (CT) state. The energy of this band matches the wide narrow emission bands observed in the luminescence spectra on the Fig. S5, indicating that radiative decay likely occurs from this CT state.

The efficiency of energy transfer processes in the investigated compounds was estimated based on experimental data and calculated using the Werts' formula[49] (Table 4). The luminescence decay curves of Eu^{3+} of complexes **1**, **3** and **5** have a monoexponential character that confirms one type of emission center in the compounds. Despite the higher overall quantum yield of complex **1** compared with complexes **3** and **5**, the non-radiative rate constant of the compounds points to the less quenching of the europium excited state in the bipyridine-containing complexes. Moreover, the luminescence lifetime of complex **1** decreases with increasing temperature, indicating the presence of temperature-stimulated quenching processes. Complex **5** demonstrates a less pronounced temperature dependence of the photophysical data while complex **3** demonstrates it complete absence. The more effective energy transfer between 4f states of Eu^{3+} in compounds **3** and **5** may be attributed to an increased pfb/1-nap ligand ratio. It was previously shown that an increase in the relative amount of the perfluorinated ligand pfb leads to a noticeable decrease in the processes of multiphonon relaxation on the high-frequency oscillators in carboxylate complexes of lanthanide ions.[43] Nevertheless, the presence of the bulky 1-nap ligand interferes with the coordination of solvent molecules. Indeed, compared with $[Eu_2(H_2O)_2(phen)_2(pfb)_6]$,[50] complex **1** exhibits a much longer luminescence lifetimes and lower non-radiative rate constant A_{nrad}.

Since the triplet levels of all coordinated ligands are located at higher energies than the excited state $^5D_0$ of Eu^{3+} ($E^{1-nap}(T_1)$ = 19 100 cm^{-1},[51] $E^{pfb}(T_1)$ = 22 300 cm^{-1},[52] $E^{phen}(T_1)$ = 22 100 cm^{-1}, and $E^{2,2'-bpy}(T_1)$ = 23 500 cm^{-1} (ref. 53)), energy transfer to the europium ion should occur from the triplet level of the ligand. The lower luminescence efficiency of complexes **3** and **5** may be result from the higher triplet level energy of 2,2′-bpy compared with phen. The energy gap between the triplet level T_1 of phen and the excited state $^5D_0$ of europium ion $\Delta E(T_1-{}^5D_0)$ = 4900 cm^{-1}, whereas for the 2,2′-bpy the energy gap $\Delta E(T_1-{}^5D_0)$ is much larger and equals to 6300 cm^{-1}. Inefficient energy transfer to the europium ion in complexes **3** and **5** is further supported by the presence of broadband luminescence, which is absent in complex **1**. The observed CT state likely contributes to the quenching of ligand excited states, thereby reducing the efficiency of europium sensitization by approximately half compared to complex **1**. The energy of the first triplet state of 1-nap is too low and close to the $^5D_1$ state of Eu^{3+}. The Sato and *et al.*[54] showed that such positioning of levels leads to low efficiency of energy transfer

Table 4 Radiative (A_{rad}) and non-radiative (A_{nrad}) rate constants, luminescence lifetimes (τ^{obs}), intrinsic ($\langle i \rangle Q^{Ln}_{Ln}$) and absolute ($Q^{Ln}_{L}$) quantum yields and sensitization efficiency (η_{sens})

Complex	A_{rad}, s^{-1}	A_{nrad}, s^{-1}	τ^{obs}, μs		Q^{Ln}_{Ln}, %	Q^{Ln}_{L}, %	η_{sens}, %
			T = 300 K	T = 77 K			
1	520	395	1090	1345	57	25	44
3	460	290	1330	1310	61	14	23
5	455	230	1460	1640	67	14	21

to the europium ion, whereas increasing $E(T_1)$ results in higher luminescence quantum yield. Such a low-lying triplet state may facilitate back energy transfer from the Eu^{3+} although the efficiency of the processes is expected to be low. Combined with the relatively high symmetry of the Eu^{3+} coordination environment of the investigation compounds, which result in a less efficient lifting of the Laporte selections rules for f–f transitions, this leads to a decrease in intrinsic quantum yield and, consequently, to a reduction in the overall luminescence quantum yield. It noteworthy that the sensitization efficiency of the complex **1** is the same as that of structurally analogous complex $[Eu_2(phen)_2(fpAc)_2(napAc)_4]\cdot 4MeCN$.[41] Since the energy level structure of the ligand environment is similar for the both complexes, the disparity in the overall luminescence efficiency arises from the differences in the radiative and non-radiative decay rates of Eu^{3+} ion. In the mixes-ligand complexes the energy transfer process typically involves interligand energy migration. This not only significantly complicates the energy transfer scheme but also creates new opportunities for enhancing luminescence efficiency. Tuning the chemical nature and relative ratios of the constituent ligands serves as a powerful method for manipulating the energy transfer channel. However, the large number of tunable parameters makes the search for optimal combinations a non-trivial task.

DFT calculations

The density functional theory method was used to calculate the structure of frontier orbitals for complexes **1–5**, **8**. The analysis of calculation results showed that the electron density in the highest occupied molecular orbital (HOMO) is predominantly localized on the 1-naphthyl ligands for all studied compounds (Fig. S7–S12).

The distribution of electron density in the lowest unoccupied molecular orbital (LUMO) can be characterized by different types. For compounds **1**, **2** and **8**: LUMO has a partial bonding character with high degree of delocalization of electron density over both europium atoms as well as the π-system of phenanthroline ligands. For compound **4**: a similar pattern of electron density distribution is observed, but with less pronounced delocalization onto the phenanthroline ligands. Additionally, carboxylic groups from pfb and 1-naphthyl ligands contribute to this delocalization. In cases of compounds **3** and **5**: LUMO acquires an antibonding nature, with predominant localization of electron density at the europium atom.

The variations in electronic structure significantly influence the fluorescence rate constants, as evidently demonstrated by the data summarized in Table 4. Specifically, when using perfluorinated pfb ligands, Table 5 reveals that the energy gap separating the singlet and triplet states diminishes considerably.

According to El-Sayed's model, the rate of intersystem crossing (ISC), between the singlet and triplet states can be described by the following equation:

$$k_{ISC} \approx (\Delta E_{ST})^{-n}, \quad n > 0$$

Table 5 Vertical excitations to the S_1 and T_1 states computed using TD-DFT, eV

	1	2	3	4	5	6	8
Singlet	2.218	2.056	1.635	1.977	1.663	2.130	1.961
Triplet	2.192	2.037	1.463	1.977	1.484	2.113	1.959

Table 6 Initial excited states following excitation, eV

	1_H	3_H	5_H
Singlet	2.025	1.834	1.871
Triplet	1.491	1.508	1.484

Therefore, the relatively large energy difference between the singlet and triplet states leads to significantly lower values of the fluorescence rate constant k_f, particularly evident for compounds **3** and **5**.

We also attempted to evaluate the contribution of transitions originating from the perfluorinated ligand (pfb) towards the benzoate anion. To this end, we replaced fluorine atoms in the investigated compounds **1**, **3** and **5** with protons and performed full optimization of the molecular structure using the DFT method (Table 6).

Comparison of the data in the tables shows that substituting protons with fluorine atoms in the benzoic acid residue significantly affects the triplet level in compound **1**, while having little effect in compounds **3** and **5**, presumably due to other dominating factors.

Conclusions

The synthetic approach developed within the framework of this study allowed precise tuning of the composition and structure of the formed mixed-anionic compounds, thus enabling the obtaining a full range of mixed-anionic 1-naphthoato-pentafluorobenzoate europium complexes. It has been demonstrated that varying the anion ratio in the composition results in a significant expansion of the structural variety in the system, leading to the formation of compounds with different nuclearities and architectures: binuclear complexes (**1–5**, **8**), cocrystals of polymer chains and binuclear molecules (**6**), and coordination polymers (**7**). One of the key factors influencing the structure and packing of the formed compounds in the crystal was the system of noncovalent interactions (π–π stacking, C–F···π, C–H···O, C–H···F, hydrogen bonding). Fine-tuning of these interactions by adjusting the anion ratio and solvents for synthesis and crystallization made it possible to control the geometry of the compounds, the spatial arrangement of ligands, and their photoluminescent properties.

The methodology, based on the interaction between a soluble carboxylate complex with an acid whose anion forms poorly soluble compounds, demonstrates potential universality for obtaining mixed-anionic carboxylate complexes with other

combinations of aromatic acids, and is also a promising tool for the rational design of brightly luminescent compounds of rare earth elements.

The use of 1-naphthaleneacetic acid also enabled analysis of the structural dependence of mixed-carboxylate complexes containing conformationally flexible substituents. It was shown that some anion positions in the obtained 1-naphthoate-pentafluorobenzoate compounds are disordered, simultaneously accommodating both 1-nap and pfb anions in varying ratios, although, compared to our previously obtained pentafluorobenzoate-benzoate compounds, the tendency toward formation of stoichiometric compositions is significantly enhanced.[55] This is likely related to the lower complementarity and substantially larger size differences between the anions used in the present study.

Luminescence studies showed that all compounds exhibit bright metal-centered luminescence, and the anion ratios in the complexes influence energy-transfer processes, primarily by activating or suppressing luminescence quenching. Based on DFT calculations of the frontier orbital structures of the obtained complexes, it was found that the relatively large energy gap between the singlet and triplet states leads to significantly lower fluorescence rate constants (k_f), which is especially characteristic for compounds **3** and **5**.

Our study deepened the understanding of the influence of substituents on the structure and optical behavior of these complexes, demonstrating that strategic engineering of the lanthanide ion's ligand environment opens up paths for developing advanced coordination compounds with outstanding photoluminescent properties.

Experimental section

Materials and methods

All reagents and solvents used for the synthesis of complexes were commercial-grade chemicals without additional purification: MeCN (>99%, KHIMMED), MeOH (99%, KHIMMED), EtOH (96%, FEREIN), C_6H_6 (>99%, KHIMMED), 1,10-phenanthroline monohydrate (phen, 99%, "Aldrich-Chemie"), 2,2′-bypiridine (2,2′-bpy, 99%, "Aldrich-Chemie"), pentafluorobenzoic acid (H(pfb), 99%, "P&M Invest"), 1-naphthoic acid (H(1-nap), 98%, "Sigma Aldrich"), 1-naphthaleneacetic acid (H(1-NAA), 98%, "Sigma Aldrich"). Starting $[Eu_2(H_2O)_8(pfb)_6]$ was synthesized using known methods.[56]

Elemental analysis was carried out on an EA1108 Carlo Erba automatic CHNS-analyzer (EuroVector, Pavia PV, Italy).

IR spectra of the compounds were recorded on a PerkinElmer Spectrum 65 spectrophotometer (PerkinElmer, Waltham, Massachusetts, United States) equipped with a Quest ATR Accessory (Specac, Orpington BR5 3FQ, United Kingdom) using attenuated total reflectance (ATR) in the range 400–4000 cm^{-1}.

The powder diffraction patterns were obtained using the Bruker D8 Advance diffractometer with a LynxEye detector in Bragg–Brentano geometry. The sample was finely dispersed on a silicon holder with a zero background, λ(CuKα) = 1.54060 Å. The acquired data were refined using the Topas 4 software.[57]

Photoluminescence excitation, emission spectra, and luminescence decays were recorded at room temperature with a Horiba–Jobin–Yvon Fluorolog-QM spectrofluorimeter equipped with a 75 W ArcTune xenon lamp and Hamamatsu R-FL-QM-R13456 photomultiplier sensitive in the 200–980 nm emission range. A cut-on longpass filter with cut-on wavelength 370 nm was used when recording the excitation and emission spectra. The luminescence quantum yield (Q_L^{Ln}) values were measured by absolute method, employing the same setup equipped with a G8 Spectralon®-covered sphere (GMP SA, Switzerland) and Hamamatsu R13456 photomultiplier. A diffusing screen was mounted inside the sphere to avoid direct irradiation of the detector. The measurements were carried out at ambient temperature. The samples in quartz cells were placed near the center of the sphere. A NIST-traceable 45 W quartz tungsten-halogen bulb emission standard (Oriel) was employed to measure the instrument response function. All QY measurements were repeated at least three times to achieve an experimental error below 15%.

Single crystal X-ray diffraction analysis of compounds was performed on a Bruker D8 Venture diffractometer equipped with a CCD detector (MoKα, λ = 0.71073 Å (for **1**, **2**, **4**, **6–8** and 7); CuKα, λ = 1.54178 Å (for **3** and **5**), graphite monochromator). A semi-empirical absorption correction using the SADABS program was applied to all compounds. Using Olex2,[58] the structure was solved with a ShelXS structure solution program using Direct Methods and refined using a ShelXL[59] refinement package with the Least Squares minimization in anisotropic approximation for nonhydrogen atoms. The H-atoms were added in the calculated positions and refined using the riding model in isotropic approximation. The occupancies of disordered pfb/1-nap anions were determined using free variables and then fixed to the nearest 0.05. The geometry of the metal polyhedra was determined using the program SHAPE 2.1.[60] The CShM coefficient represents the deviation of atomic coordinates in the coordination environment of the metal ion from the vertices of an ideal polyhedron. A CShM value of 0 indicates perfect correspondence between the polyhedral geometry and the ideal polyhedron.

Crystallographic parameters and refinement details are presented in Tables S1 and S2, with the main bond lengths and angles given in Tables 1 and 3. Table S3 contains CShM values. Principal intra- and intermolecular interaction distances and angles are listed in Tables 2, S4 and S5. CCDC 2484403 (**1**), 2470581 (**2**), 2470583 (**3**), 2470582 (**4**), 2470585 (**5**), 2470586 (**6**), 2484404 (**7·MeCN**), 2484413 (**7·MeOH**), 2470587 (**8**) contain the supplementary crystallographic data for this paper.

Quantum chemical calculations were performed using the ORCA 6.0 program pack.[61] Geometries and vibration spectra were calculated using DFT in a TZ + 2P basis set, including D4 dispersion and geometry counterpoise corrections (r2SCAN-3c/D4/def2-mTZVPP).[62–64] A search for stationary points on potential energy surfaces was performed by full geo-

metry optimization using the TightSCF and TightOpt convergence criteria. Analytical calculations of harmonic frequencies were used to obtain thermodynamic quantities and to verify that all found stationary points are local minima. The thermodynamic quantities were calculated in the harmonic approximation harmonic oscillator-rigid rotor. The investigation of electron density distribution on frontier orbitals and transition energies was carried out by means of a single-point calculation utilizing the time-dependent version of the density functional theory described above.

Synthesis of complexes

Synthesis of $[Eu_2(phen)_2(1\text{-nap})_4(pfb)_2]\cdot 2MeCN$ (1). The H(1-nap) (0.021 g, 0.12 mmol) was added to $[Eu_2(H_2O)_8(pfb)_6]\cdot 2H_2O$ (0.05 g, 0.03 mmol) in 8 mL of EtOH and 30 mL of MeCN, and the mixture was stirred at 60 °C for 1 hour to complete dissolution of the reagents. 1,10-Phenanthroline (0.011 g, 0.06 mmol) was added, and the mixture was stirred for an additional 10 minutes without heating. The colorless solution was allowed to evaporate slowly at room temperature. After one and a half month, colorless crystals, suitable for X-ray diffraction were isolated by decantation, washed with cold MeOH ($T \approx 5$ °C), and then dried in air. The yield of 1 was 0.021 g (38%) based on $[Eu_2(H_2O)_8(pfb)_6]$. Found, %: C 55.8; H 2.6; N 4.5. For $C_{86}H_{50}N_6O_{12}F_{10}Eu_2$ calculated, %: C 55.7; H 2.7; N 4.5. IR(ATR), ν/cm^{-1}: 3050 w, 1629 s, 1577 m, 1519 s, 1506 m, 1458 m, 1407 s, 1375 s, 1345 m, 1295 w, 1257 w, 1219 w, 1142 w, 1105 m, 1029 w, 992 m, 873 m, 863 w, 845 m, 822 w, 785 s, 768 s, 742 m, 727 s, 651 m, 639 m, 583 w, 567 w, 557 w.

Synthesis of $[Eu_2(H_2O)_2(phen)_2(1\text{-nap})_2(pfb)_4]\cdot 2MeCN$ (2). H (1-nap) (0.015 g, 0.09 mmol) was added to $[Eu_2(H_2O)_8(pfb)_6]\cdot 2H_2O$ (0.05 g, 0.03 mmol) in 8 mL of EtOH and 30 mL of MeCN, and the mixture was stirred at 60 °C for 1 hour to complete dissolution of the reagents. 1,10-Phenanthroline (0.011 g, 0.06 mmol) was added, and the mixture was stirred for an additional 10 minutes without heating. The colorless solution was allowed to evaporate slowly at room temperature. After one and a half month, colorless crystals, suitable for X-ray diffraction were isolated by decantation, washed with cold MeOH ($T \approx 5$ °C), and then dried in air. The yield of **2** was 0.018 g (31%) based on $[Eu_2(H_2O)_8(pfb)_6]$. Found, %: C 47.7; H 1.6; N 4.0. For $C_{78}H_{40}N_6O_{14}F_{20}Eu_2$ calculated, %: C 47.6; H 2.0; N 4.3. IR(ATR), ν/cm^{-1}: 3854 w, 3749 w, 3649 w, 3434 w, 3059 w, 2973 w, 2898 w, 1683 m, 1629 s, 1578 s, 1550 m, 1519 s, 1505 s, 1458 m, 1406 s, 1376 s, 1345 m, 1295 w, 1257 w, 1220 w, 1141 w, 1104 m, 1080 m, 1046 s, 992 s, 929 m, 875 w, 863 m, 847 m, 831 w, 822 w, 786 s, 768 s, 742 m, 728 s, 721 m, 659 m, 651 m, 635 m, 592 m, 582 m.

Synthesis of $[Eu_2(2,2'\text{-bpy})_2(1\text{-nap})_2(pfb)_4]\cdot 2MeCN$ (3) and $[Eu_2(2,2'\text{-bpy})_2(1\text{-nap})_3(pfb)_3]\cdot 2MeCN$ (4). H(1-nap) (0.031 g, 0.18 mmol) was added to $[Eu_2(H_2O)_8(pfb)_6]\cdot 2H_2O$ (0.1 g, 0.06 mmol) in 10 mL of MeOH and 50 mL of MeCN, and the mixture was stirred at 60 °C for 1 hour to complete dissolution of the reagents. 2,2′-Bipyridine (0.019 g, 0.12 mmol) was added, and the mixture was stirred for an additional 10 minutes without heating. The colorless solution was allowed to evaporate slowly at room temperature. After 35 days, colorless crystals of **3**, suitable for X-ray diffraction were isolated by decantation, washed with cold MeOH ($T \approx 5$ °C) and then dried in air. Further slow evaporation of the mother liquor for a week yielded both **3** and **4**, which were isolated by decantation, washed with cold MeOH ($T \approx 5$ °C), and then dried in air. The yield of **3** was 0.012 g (22%) based on $[Eu_2(H_2O)_8(pfb)_6]$. Found for 3, %: C 47.1; H 2.0; N 4.6. For $C_{74}H_{36}N_6O_{12}F_{20}Eu_2$ calculated, %: C 47.2; H 1.9; N 4.5. IR(ATR) for 3, ν/cm^{-1}: 3854 w, 3748 w, 3671 w, 3525 w, 2943 w, 2293 w, 2253 w, 1732 w, 1716 w, 1698 w, 1651 w, 1595 m, 1579 m, 1554 s, 1522 s, 1509 s, 1490 m, 1404 m, 1375 s, 1361 s, 1339 m, 1292 w, 1261 w, 1213 w, 1151 w, 1111 w, 1024 s, 1007 s, 936 m, 919 w, 879 m, 827 w, 814 w, 781 s, 751 s, 659 m, 584 m.

Synthesis of $[Eu_2(2,2'\text{-bpy})_2(1\text{-nap})_2(pfb)_4]\cdot 2C_6H_6$ (5). H(1-nap) (0.016 g, 0.09 mmol) was added to $[Eu_2(H_2O)_8(pfb)_6]\cdot 2H_2O$ (0.05 g, 0.03 mmol) in 8 mL of MeOH and 30 mL of MeCN, and the mixture was stirred at 60 °C for 1 hour to complete dissolution of the reagents. 2,2′-Bipyridine (0.009 g, 0.06 mmol) was added, and the mixture was stirred for an additional 10 minutes without heating. After cooling the reaction mixture to ambient temperature, 14 mL of benzene was added. The colorless solution was allowed to evaporate slowly at room temperature. After 15 days, colorless crystals, suitable for X-ray diffraction were isolated by decantation, washed with cold MeOH ($T \approx 5$ °C), and then dried in air. The yield of 5 was 0.026 g (45%) based on $[Eu_2(H_2O)_8(pfb)_6]$. Found, %: C 50.4; H 2.0; N 3.0. For $C_{82}H_{42}N_4O_{12}F_{20}Eu_2$ calculated, %: C 50.3; H 2.2; N 2.9. IR(ATR), ν/cm^{-1}: 3854 w, 3735 w, 3672 w, 3648 w, 2986 w, 2360 w, 1683 m, 1644 s, 1626 s, 1520 s, 1489 s, 1457 m, 1412 s, 1378 s, 1321 m, 1292 m, 1255 m, 1157 w, 1105 m, 1063 w, 991 s, 943 m, 927 m, 875 m, 828 m, 789 m, 768 s, 740 s, 699 m, 682 m, 658 m, 644 m, 624 w, 582 w.

Synthesis of $[Eu_4(phen)_4(1\text{-nap})_1(pfb)_{11}]_n\cdot n[Eu_2(phen)_2(1\text{-nap})_{2.7}(pfb)_{3.3}]$ (6). H(1-nap) (0.010 g, 0.06 mmol) was added to $[Eu_2(H_2O)_8(pfb)_6]\cdot 2H_2O$ (0.05 g, 0.03 mmol) in 8 mL of EtOH and 35 mL of MeCN, and the mixture was stirred at 60 °C for 1 hour to complete dissolution of the reagents. 1,10-Phenanthroline (0.011 g, 0.06 mmol) was added, and the mixture was stirred for an additional 10 minutes without heating. The colorless solution was allowed to evaporate slowly at room temperature. After 35 days, colorless crystals, suitable for X-ray diffraction were isolated by decantation, washed with cold MeOH ($T \approx 5$ °C), and then dried in air. The yield of 6 was 0.20 g (36%) based on $[Eu_2(H_2O)_8(pfb)_6]$. Found, %: C 45.2; H 1.4; N 3.2. For $C_{218.8}H_{73.9}N_{12}O_{36}F_{71.5}Eu_6$ calculated, %: C 45.3; H 1.3; N 3.0. IR(ATR), ν/cm^{-1}: 3854 w, 3838 w, 3819 w, 3801 w, 3748 w, 3690 w, 3671 w, 3648 w, 3629 w, 3566 w, 2987 w, 2360 w, 1732 w, 1698 w, 1683 w, 1646 w, 1625 s, 1558 m, 1540 m, 1507 s, 1489 s, 1456 m, 1415 m, 1377 m, 1257 w, 1155 w, 1105 m, 1067 m, 992 s, 928 m, 875 m, 841 w, 827 w, 792 m, 768 m, 741 m, 683 w, 658 w, 584 w, 566 w, 555 w.

Synthesis of mixture $[Eu_2(phen)_2(pfb)_6]_n\cdot 2MeCN$ (7·MeCN) and $[Eu_2(phen)_2(pfb)_6]_n\cdot 4MeOH$ (7·MeOH). 1,10-Phenanthroline

(0.011 g, 0.06 mmol) was added to $[Eu_2(H_2O)_8(pfb)_6]\cdot 2H_2O$ (0.05 g, 0.03 mmol) in 5 mL of MeOH and 10 mL of MeCN, and the mixture was stirred at 60 °C for 3 hours to complete dissolution of the reagents. The colorless solution was allowed to evaporate slowly at room temperature. After 10 days, colorless crystals, suitable for X-ray diffraction were isolated by decantation, washed with cold MeOH ($T \approx 5$ °C), and then dried in air. IR(ATR), ν/cm^{-1}: 3648 w, 2159 w, 1699 w, 1616 s, 1520 m, 1488 s, 1394 s, 1350 w, 1299 w, 1142 w, 1060 w, 1005 s, 990 s, 931 m, 864 m, 838 m, 768 s, 740 m, 727 m, 695 w, 639 w, 583 w, 566 w, 558 w.

Synthesis of $[Eu_2(phen)_2(1\text{-}NAA)_2(pfb)_4]$ (8). H(1-NAA) (0.017 g, 0.09 mmol) was added to $[Eu_2(H_2O)_8(pfb)_6]\cdot 2H_2O$ (0.05 g, 0.03 mmol) in 10 mL of EtOH and 10 mL of MeCN, and the mixture was stirred at 60 °C for 1 hour to complete dissolution of the reagents. 1,10-Phenanthroline (0.011 g, 0.06 mmol) was added, and the mixture was stirred for an additional 10 minutes without heating. The colorless solution was allowed to evaporate slowly at room temperature. After 5 days, colorless crystals, suitable for X-ray diffraction were isolated by decantation, washed with cold MeOH ($T \approx 5$ °C), and then dried in air. The yield of **8** was 0.018 g (32%) based on $[Eu_2(H_2O)_8(pfb)_6]$. Found, %: C 48.7; H 1.6; N 3.0. For $C_{76}H_{34}N_4O_{12}F_{20}Eu_2$ calculated, %: C 48.6; H 1.8; N 3.0. IR (ATR), ν/cm^{-1}: 3854 w, 3838 w, 3819 w, 3801 w, 3748 w, 3566 w, 2987 w, 2253 w, 1732 w, 1716 w, 1698 w, 1648 w, 1627 m, 1598 s, 1518 m, 1487 m, 1423 s, 1402 s, 1290 m, 1258 w, 1232 w, 1140 w, 1104 m, 1040 m, 993 s, 918 m, 862 w, 846 m, 829 w, 777 s, 766 m, 743 m, 729 m, 629 w, 584 w.

Author contributions

Conceptualization, validation, A. A. L., J. K. V.; methodology, M. A. S., A. S. C., E. A. V.; formal analysis, A. A. L., M. A. S., A. S. C., E. A. V., I. V. T., A. V. L; investigation, A. A. L., M. A. S., A. S. C., E. A. V.; writing – original draft preparation M. A. S., A. S. C., A. V. L.; writing – review and editing, A. A. S., J. K. V., A. V. L, I. L. E.; supervision, I. L. E. All authors have read and agreed to the published version of the manuscript.

Conflicts of interest

There are no conflicts to declare.

Data availability

The data supporting this article have been included as part of the supplementary information (SI). Supplementary information: crystallographic parameters and refinement details are presented in Tables S1 and S2, with the main bond lengths and angles given in Tables 1 and 3. Table S3 contains CShM values. Principal intra- and intermolecular interaction distances and angles are listed in Tables 2, S4 and S5. See DOI: https://doi.org/10.1039/d5dt02665b.

CCDC 2484403 (**1**), 2470581 (**2**), 2470583 (**3**), 2470582 (**4**), 2470585 (**5**), 2470586 (**6**), 2484404 (**7·MeCN**), 2484413 (**7·MeOH**), 2470587 (**8**) contain the supplementary crystallographic data for this paper.[65a–i]

Acknowledgements

The study was supported by the Russian Science Foundation grant No. 25-73-10110, https://rscf.ru/en/project/25-73-10110/. IR spectroscopy, X-ray diffraction, powder X-ray diffraction and CHN analyses of the complexes were performed using the equipment of the JRC PMR IGIC RAS as part of the state assignment of the IGIC RAS in the field of fundamental scientific research. Photophysical measurements were carried out with financial support from the Ministry of Science and Higher Education of the Russian Federation, using the equipment of the Research Center for Molecular Structure Studies, INEOS RAS.

References

1 C. D. Brites, R. Marin, M. Suta, A. N. Carneiro Neto, E. Ximendes, D. Jaque and L. D. Carlos, Spotlight on luminescence thermometry: basics, challenges, and cutting–edge applications, *Adv. Mater.*, 2023, **35**(36), 2302749.
2 J. Mondal, R. Lamba, Y. Yukta, R. Yadav, R. Kumar, B. Pani and B. Singh, Advancements in semiconductor quantum dots: expanding frontiers in optoelectronics, analytical sensing, biomedicine, and catalysis, *J. Mater. Chem. C*, 2024, **12**(28), 10330–10389.
3 J. Li, X. Zhao and X. Gong, The emerging star of carbon luminescent materials: exploring the mysteries of the nanolight of carbon dots for optoelectronic applications, *Small*, 2024, **20**(31), 2400107.
4 N. Thanjavur, L. Bugude and Y. J. Kim, Integration of functional materials in photonic and optoelectronic technologies for advanced medical diagnostics, *Biosensors*, 2025, **15**(1), 38.
5 A. S. Manna, S. Ghosh, T. Ghosh, N. Karchaudhuri, S. Das, A. Roy and D. K. Maiti, Smart luminescent materials for emerging sensors: Fundamentals and advances, *Chem. – Asian J.*, 2025, **20**(6), e202401328.
6 W. R. Algar, M. Massey, K. Rees, R. Higgins, K. D. Krause, G. H. Darwish, G. H. Darwish, W. J. Peveler, Z. Xiao, H.-Y. Tsai, R. Gupta, K. Lix, M. V. Tran and H. Kim, Photoluminescent nanoparticles for chemical and biological analysis and imaging, *Chem. Rev.*, 2021, **121**(15), 9243–9358.
7 H. H. Li, Y. K. Wang and L. S. Liao, Near–infrared luminescent materials incorporating rare earth/transition metal ions: from materials to applications, *Adv. Mater.*, 2024, **36**(30), 2403076.
8 A. de Bettencourt-Dias, *Luminescence of lanhanide ions in coordination compounds and nanomaterials*, John Wiley and Sons, Ltd, West Sussex, United Kingdom, 2014.

9 G. Tessitore, G. A. Mandl, S. L. Maurizio, M. Kaur and J. A. Capobianco, The role of lanthanide luminescence in advancing technology, *RSC Adv.*, 2023, **13**(26), 17787–17811.
10 S. Wang, B. Sun, Z. Su, G. Hong, X. Li, Y. Liu, Q. Pan and J. Sun, Lanthanide-MOFs as multifunctional luminescent sensors, *Inorg. Chem. Front.*, 2022, **9**(13), 3259–3266.
11 B. Yan, Luminescence response mode and chemical sensing mechanism for lanthanide-functionalized metal–organic framework hybrids, *Inorg. Chem. Front.*, 2021, **8**(1), 201–233.
12 M. Rizwan, K. Zaman, S. Ahmad, A. Ayub and M. Tanveer, *Rare–Earth Ions in Solid–State Devices*. *Quantum Optics Devices on a Chip*, John Wiley and Sons, Ltd, West Sussex, United Kingdom, 2025.
13 Y. Yang, X. Hu, Z. Yang and W. Huang, Insights into molecular lanthanide complexes: construction, properties and bioimaging and biosensing applications, *Adv. Funct. Mater.*, 2025, **35**(2), 2412970.
14 X. Zhai, Y. Kou, L. Liang, P. Liang, P. Su and Y. Tang, AIE ligand-based luminescent Ln-MOFs for rapid and selective sensing of tetracycline, *Inorg. Chem.*, 2023, **62**(45), 18533–18542.
15 M. A. Shmelev, N. V. Gogoleva, V. K. Ivanov, V. V. Kovalev, G. A. Razgonyaeva, M. A. Kiskin, A. A. Sidorov and I. L. Eremenko, Heterometallic Ln(III)–Cd(II) complexes with anions of monocarboxylic acids: Synthetic approaches and analysis of structures and photoluminescence properties, *Russ. J. Coord. Chem.*, 2022, **48**(9), 539–556.
16 M. A. Shmelev, S. N. Melnikov, S. A. Nikolaevskii, S. R. Kiraev, I. V. Ananyev, Y. V. Nelyubina, E. A. Varaksina, V. M. Korshunov, I. V. Taydakov, A. S. Goloveshkin, N. V. Gogoleva, A. A. Sidorov, I. L. Eremenko and M. A. Kiskin, Effect of the Introduction of ZnII and CdII Ions on EuIII and TbIII Emission in M_2Ln_2 Heterometallic Molecules With 2–Furoic Acid Anions, *Appl. Organomet. Chem.*, 2025, **39**(2), e7836.
17 D. Parker, J. D. Fradgley and K. L. Wong, The design of responsive luminescent lanthanide probes and sensors, *Chem. Soc. Rev.*, 2021, **50**(14), 8193–8213.
18 P. A. Tanner, W. Thor, Y. Zhang and K. L. Wong, Energy transfer mechanism and quantitative modeling of rate from an antenna to a lanthanide ion, *J. Phys. Chem. A*, 2022, **126**(41), 7418–7431.
19 N. A. Avagyan, P. S. Lemport, T. A. Polikovskiy, A. V. Tsorieva, M. T. Metlin, I. V. Taydakov, R. V. Zonov, K. A. Lyssenko, M. F. Vokuev, I. A. Rodin, V. A. Roznyatovsky, Y. A. Ustynyuk and V. G. Nenajdenko, Large energy gap between singlet and triplet states is no longer a problem: intermediate charge transfer state boosts overall quantum yield up to 67% in Eu3 + complexes, *Rare Met.*, 2025, **44**(6), 4279–4293.
20 J. D. L. Dutra, W. F. Oliveira, G. S. Silva, T. D. Bispo and R. O. Freire, LUMPAC 2.0—Bridging Theory and Experiment in the Study of Luminescent Systems, *J. Comput. Chem.*, 2025, **46**(17), e70143.
21 E. D. Boltkov, M. E. Buzoverov, E. K. Lermontova, Y. A. Belousov, D. A. Steshenko, V. E. Gontcharenko and T. Y. Glazunova, The miracle of self-assembly: a journey of the $\{Ln_6F_8\}$ core in the world of lanthanides, *Dalton Trans.*, 2025, **54**(33), 12503–12515.
22 X. Z. Li, C. B. Tian and Q. F. Sun, Coordination-directed self-assembly of functional polynuclear lanthanide supramolecular architectures, *Chem. Rev.*, 2022, **122**(6), 6374–6458.
23 J. Li, Y. Zhao, D. Yu and C. Zhan, Recent Advances in d–f Transition Lanthanide Complexes for Organic Light–Emitting Diodes: Insights into Structure–Luminescence Relationships, *Laser Photonics Rev.*, 2025, 2402198.
24 J. K. Voronina, D. S. Yambulatov, A. S. Chistyakov, A. E. Bolot'ko, L. M. Efromeev, M. A. Shmelev, A. A. Sidorov and I. L. Eremenko, Influence of the Arene/Perfluoroarene Ratio on the Structure and Non-Covalent Interactions in Crystals of Cd(II), Cd(II)-Tb(III) and Cu(II) Compounds, *Crystals*, 2023, **13**(4), 678.
25 M. Mehmood, A. Zafar, A. Iqbal, M. Mukhtar and M. N. Tahir, Molecular architecture, characterization, and applications of homoleptic heteronuclear 3d/4f metals' complexes derived from bi-compartmental Schiff-base, *J. Mol. Struct.*, 2023, **1274**, 134547.
26 Y. M. Wang, Y. Wang, R. X. Wang, J. Q. Qiu, Y. X. Chi, J. Jin and S. Y. Niu, Syntheses, structures and photophysical properties of a series of Zn-Ln complexes, *J. Phys. Chem. Solids*, 2017, **104**, 221–227.
27 M. A. Shmelev, N. V. Gogoleva, A. A. Sidorov, Y. A. Nelyubina, F. M. Dolgushin, Y. K. Voronina, M. A. Kiskin, G. G. Aleksandrov, E. A. Varaksina, I. V. Taydakov and I. L. Eremenko, Chemical Assembling of Heterometallic {Cd–M} (M=Li, Mg, Eu, Tb) Molecules with 3,5-Di-tert-butylbenzoate Bridges and N-Donor Ligands, *ChemistrySelect*, 2020, **5**(28), 8475–8482.
28 J. Manzur, P. Fuentealba, Y. Gil, J. Pérez-Obando, J. Morales Alfaro, A. I. Vega Carvallo, D. Aravena, R. C. de Santana, A. N. Carneiro Neto and E. Spodine, Tuning the emission of homometallic DyIII, TbIII, and EuIII 1-D coordination polymers with 2, 6-di (1 H-1, 2, 4-triazole-1-yl-methyl)-4-R-phenoxo ligands: sensitization through the singlet state, *Inorg. Chem.*, 2023, **62**(47), 19195–19207.
29 N. A. Avagyan, P. S. Lemport, T. A. Polikovskiy, A. V. Tsorieva, M. T. Metlin, I. V. Taydakov, R. V. Zonov, K. A. Lyssenko, M. F. Vokuev, I. A. Rodin, V. A. Roznyatovsky, Y. A. Ustynyuk and V. G. Nenajdenko, Large energy gap between singlet and triplet states is no longer a problem: intermediate charge transfer state boosts overall quantum yield up to 67% in Eu3 + complexes, *Rare Met.*, 2025, **44**(6), 4279–4293.
30 N. K. Kalluvettukuzhy, M. R. Maciejczyk and N. Robertson, Thermally activated delayed fluorescence emitters for efficient sensitization of europium(III), *Phys. Chem. Chem. Phys.*, 2024, **26**(26), 18129–18137.
31 P. J. Wright, M. C. Pfrunder, I. M. Etchells, M. A. Haghighatbin, P. Raiteri, M. I. Ogden, S. Stagni,

C. F. Hogan, L. J. Cameron, E. G. Moore and M. Massi, Elucidating the Mechanism of Efficient Eu(III) and Yb(III) Sensitisation from a Re(I) Tetrazolato Triangular Assembly, *Chem. – Eur. J.*, 2024, **30**(49), e202401233.

32 M. Bazi, M. Tomassoni, L. Bellucci, G. Bottaro, M. Rancan, S. Samaritani, L. Armelao and L. Labella, Heteronuclear Eu 2 Pt 2 luminescent arrays: composition–thermometric properties correlations, *Inorg. Chem. Front.*, 2025, **12**, 6257–6273.

33 J. J. Zakrzewski, B. Sieklucka and S. Chorazy, Europium(III) photoluminescence governed by d8–d10 heterometallophilic interactions in trimetallic cyanido-bridged coordination frameworks, *Inorg. Chem.*, 2020, **59**(2), 1393–1404.

34 M. Wyczesany, J. J. Zakrzewski, B. Sieklucka and S. Chorazy, Metal-cyanido molecular modulators of the sensing range and performance in lanthanide-based luminescent thermometers, *J. Mater. Chem. C*, 2022, **10**(33), 12054–12069.

35 S. P. Panguluri, E. Jourdain, P. Chakraborty, S. Klyatskaya, M. M. Kappes, A. M. Nonat, L. J. Charbonnière and M. Ruben, Yb-to-Eu cooperative sensitization upconversion in a multifunctional molecular nonanuclear lanthanide cluster in solution, *J. Am. Chem. Soc.*, 2024, **146**(19), 13083–13092.

36 D. Avram, C. Colbea, A. A. Patrascu, M. C. Istrate, V. Teodorescu and C. Tiseanu, Up-conversion emission in transition metal and lanthanide co-doped systems: dimer sensitization revisited, *Sci. Rep.*, 2023, **13**(1), 2165.

37 Q. F. Li, L. Zhang, M. Shen, J. T. Wang, L. Jin and Z. Wang, Photochromic diarylethene induced fluorescence switching materials constructed by non-covalent interactions, *J. Mater. Chem. C*, 2023, **11**(38), 12828–12847.

38 A. Haque, K. M. Alenezi, M. S. Khan, W. Y. Wong and P. R. Raithby, Non-covalent interactions (NCIs) in π-conjugated functional materials: advances and perspectives, *Chem. Soc. Rev.*, 2023, **52**(2), 454–472.

39 W. L. Zhou, Y. Chen, W. Lin and Y. Liu, Luminescent lanthanide–macrocycle supramolecular assembly, *Chem. Commun.*, 2021, **57**(87), 11443–11456.

40 M. A. Shmelev, J. K. Voronina, M. A. Evtyukhin, F. M. Dolgushin, E. A. Varaksina, I. V. Taydakov, A. A. Sidorov, I. L. Eremenko and M. A. Kiskin, Synthesis, structure and photoluminescence properties of Cd and Cd-Ln pentafluorobenzoates with 2, 2′: 6′, 2′-terpyridine derivatives, *Inorganics*, 2022, **10**(11), 194.

41 A. A. Levina, A. S. Chistyakov, M. A. Shmelev, E. A. Varaksina, J. K. Voronina, N. V. Gogoleva, I. V. Taydakov, A. A. Sidorov and I. L. Eremenko, Effects of combining fluorinated and non-fluorinated monocarboxylate anions in lanthanide complexes on the structure and photoluminescence properties, *New J. Chem.*, 2025, **49**(30), 12959–12970.

42 A. E. Bolot'ko, M. A. Shmelev, A. S. Chistyakov, J. K. Voronina, E. A. Varaksina, N. V. Gogoleva, I. V. Taydakov, A. A. Sidorov and I. L. Eremenko, Luminescence enhancement by mixing carboxylate benzoate–pentafluorobenzoate ligands in polynuclear $\{Eu_2Zn_2\}$ and $\{Tb_2Zn_2\}$ complexes, *Dalton Trans.*, 2025, **54**(14), 5708–5720.

43 M. A. Shmelev, A. A. Levina, A. S. Chistyakov, E. A. Varaksina, J. K. Voronina, G. A. Razgonyaeva, I. V. Taidakov, A. A. Sidorov and I. L. Eremenko, Influence of the anion ratio in the composition of mixed benzoate/pentafluorobenzoate complexes of europium on the structure and photoluminescent properties, *Mendeleev Commun.*, 2025, **35**(1), 35–38.

44 N. V. Gogoleva, M. A. Shmelev, A. S. Chistyakov, G. A. Razgonyaeva, V. M. Korshunov, A. V. Tsorieva, I. V. Taydakov, A. A. Sidorov and I. L. Eremenko, Synthesis, structure, and photoluminescent properties of a mixed carboxylate pentafluorobenzoate–phenylacetate complex of terbium, *Mendeleev Commun.*, 2024, **34**(4), 484–487.

45 M. A. Shmelev, G. N. Kuznetsova, N. V. Gogoleva, F. M. Dolgushin, Y. V. Nelyubina, M. A. Kiskin, A. A. Sidorov and I. L. Eremenko, Heteroleptic cadmium(II) and terbium(III) pentafluorobenzoate-benzoate and pentafluorobenzoate-2-furancarboxylate compounds, *Russ. Chem. Bull.*, 2021, **70**(5), 830–838.

46 S. P. Yang, H. Yang, X. B. Yu and Z. M. Wang, Synthesis, structure and fluorescence of Eu2 (NAP) 6 (PHEN) 2 (NAPH= α-naphthoic acid; PHEN= 1, 10-phenanthroline), *J. Mol. Struct.*, 2003, **659**(1–3), 97–102.

47 K. Binnemans, Interpretation of europium(III) spectra, *Coord. Chem. Rev.*, 2015, **295**, 1–45.

48 V. Tsaryuk, K. Lyssenko, K. Zhuravlev, V. Zolin, V. Kudryashova, I. Pekareva and Z. Klemenkova, Influence of ligand architecture on the structure of coordination centre in dimeric europium carboxylates with 1, 10-phenanthroline, *J. Rare Earths*, 2009, **27**(4), 539–543.

49 M. H. Werts, R. T. Jukes and J. W. Verhoeven, The emission spectrum and the radiative lifetime of Eu^{3+} in luminescent lanthanide complexes, *Phys. Chem. Chem. Phys.*, 2002, **4**(9), 1542–1548.

50 L. J. Han, Y. J. Kong, N. Sheng and X. L. Jiang, A new europium fluorous metal–organic framework with pentafluorobenzoate and 1, 10-phenanthroline ligands: Synthesis, structure and luminescent properties, *J. Fluor. Chem.*, 2014, **166**, 122–126.

51 M. Hilder, P. C. Junk, U. H. Kynast and M. M. Lezhnina, Spectroscopic properties of lanthanoid benzene carboxylates in the solid state: Part 1, *J. Photochem. Photobiol., A*, 2009, **202**(1), 10–20.

52 E. A. Mikhalyova, A. V. Yakovenko, M. Zeller, K. S. Gavrilenko, M. A. Kiskin, S. S. Smola, V. P. Dotsenko, I. L. Eremenko, A. W. Addison and V. V. Pavlishchuk, Crystal structures and intense luminescence of tris (3-(2′-pyridyl)-pyrazolyl) borate Tb^{3+} and Eu^{3+} complexes with carboxylate co-ligands, *Dalton Trans.*, 2017, **46**(11), 3457–3469.

53 Z. V. Dobrokhotova, S. P. Petrosyants, A. B. Ilyukhin, Y. S. Zavorotny, V. I. Gerasimova, Y. A. Mikhlina,

N. N. Efimov and V. M. Novotortsev, New neutral and anionic thiocyanate complexes of Y(III) and Eu(III) with 2,2′-bipyridine and 1,10-phenanthroline: Synthesis, structures, thermal behavior and photophysical properties, *Inorg. Chim. Acta*, 2017, **456**, 76–85.

54 S. Sato and M. Wada, Relations between intramolecular energy transfer efficiencies and triplet state energies in rare earth β-diketone chelates, *Bull. Chem. Soc. Jpn.*, 1970, **43**(7), 1955–1962.

55 A. E. Bolot'ko, M. A. Shmelev, A. A. Bovkunova, A. A. Sidorov and I. L. Eremenko, Effect of the Nature of N-Donor Ligands on the Structure of Mixed-Anion Europium Benzoate Pentafluorobenzoate Compounds, *Russ. J. Coord. Chem.*, 2025, **51**(10), 886.

56 S. V. Larionov, L. A. Glinskaya, T. G. Leonova, R. F. Klevtsova, E. M. Uskov, V. E. Platonov, V. M. Karpov and V. P. Fadeeva, Luminescence properties of complexes Ln (Phen)$(C_6F_5COO)_3$ (Ln= Tb, Eu) and Ln $(C_6F_5COO)_3\cdot nH_2O$ (Ln= Tb, n= 2; Ln= Eu, n= 1). Structures of the $[Tb_2(H_2O)_8(C_6F_5COO)_6]$ complex and its isomer in the supramolecular compound $[Tb_2(H_2O)_8(C_6F_5COO)_6]\cdot 2C_6F_5COOH$, *Russ. J. Coord. Chem.*, 2009, **35**(11), 798–806.

57 N. V. Y. Scarlett and I. C. Madsen, Quantification of phases with partial or no known crystal structures, *Powder Diffr.*, 2006, **21**(4), 278.

58 O. V. Dolomanov, L. J. Bourhis, R. J. Gildea, J. A. K. Howard and H. Puschmann, OLEX2: a complete structure solution, refinement and analysis program, *J. Appl. Crystallogr.*, 2009, **42**, 339.

59 G. M. Sheldrick, Crystal structure solution with ShelXT, *Acta Crystallogr., Sect. C: Struct. Chem.*, 2015, **71**, 3.

60 D. Casanova, M. Llunell, P. Alemany and S. Alvarez, The rich stereochemistry of eight–vertex polyhedra: a continuous shape measures study, *Chem. – Eur. J.*, 2005, **11**, 1479.

61 F. Neese, Software update: the ORCA program system, version 5.0, *WIREs Comput. Mol. Sci.*, 2022, **12**(1), e1606.

62 S. Grimme, A. Hansen, S. Ehlert and J. Mewes, r2SCAN-3c: A 'Swiss army knife' composite electronic-structure method, *J. Chem. Phys.*, 2021, **154**, 064103.

63 J. W. Furness, A. D. Kaplan, J. Ning, J. P. Perdew and J. Sun, Accurate and Numerically Efficient r2SCAN Meta-Generalized Gradient Approximation, *J. Phys. Chem. Lett.*, 2020, **11**, 8208–8215.

64 F. Neese, An improvement of the resolution of the identity approximation for the formation of the Coulomb matrix, *J. Comput. Chem.*, 2003, **24**(14), 1740–1747.

65 (*a*) CCDC 2484403: Experimental Crystal Structure Determination, 2025, DOI: 10.5517/ccdc.csd.cc2pd71d; (*b*) CCDC 2470581: Experimental Crystal Structure Determination, 2025, DOI: 10.5517/ccdc.csd.cc2nxv5m; (*c*) CCDC 2470583: Experimental Crystal Structure Determination, 2025, DOI: 10.5517/ccdc.csd.cc2nxv7p; (*d*) CCDC 2470582: Experimental Crystal Structure Determination, 2025, DOI: 10.5517/ccdc.csd.cc2nxv6n; (*e*) CCDC 2470585: Experimental Crystal Structure Determination, 2025, DOI: 10.5517/ccdc.csd.cc2nxv9r; (*f*) CCDC 2470586: Experimental Crystal Structure Determination, 2025, DOI: 10.5517/ccdc.csd.cc2nxvbs; (*g*) CCDC 2484404: Experimental Crystal Structure Determination, 2025, DOI: 10.5517/ccdc.csd.cc2pd72f; (*h*) CCDC 2484413: Experimental Crystal Structure Determination, 2025, DOI: 10.5517/ccdc.csd.cc2pd7cq; (*i*) CCDC 2470587: Experimental Crystal Structure Determination, 2025, DOI: 10.5517/ccdc.csd.cc2nxvct.